View Article Online / Journal Homepage / Table of Contents for this issue
Dynamic Article Links

Nanoscale

Cite this: *Nanoscale*, 2012, **4**, 5277

www.rsc.org/nanoscale

FEATURE ARTICLE

Recent advances in transformation optics

Yongmin Liu[a] and Xiang Zhang*[ab]

Received 9th May 2012, Accepted 27th June 2012
DOI: 10.1039/c2nr31140b

Within the past a few years, transformation optics has emerged as a new research area, since it provides a general methodology and design tool for manipulating electromagnetic waves in a prescribed manner. Using transformation optics, researchers have demonstrated a host of striking phenomena and devices; many of which were only thought possible in science fiction. In this paper, we review the most recent advances in transformation optics. We focus on the theory, design, fabrication and characterization of transformation devices such as the carpet cloak, "Janus" lens and plasmonic cloak at optical frequencies, which allow routing light at the nanoscale. We also provide an outlook of the challenges and future directions in this fascinating area of transformation optics.

1. Introduction

Nobody would disagree that the better understanding, manipulation and application of light, or electromagnetic waves in a more general respect, play a crucial role in advancing science and technology. The underlying driving force is the long-standing interest and attention of human beings concerning novel electromagnetic phenomena and devices. Without persistent pursuits, it is impossible to develop a more efficient and directional radar antenna, a brighter light source, or an instrument with higher imaging resolution. One of the central aims of these devices is to control and direct electromagnetic fields. For instance, by optimizing the curvature of glass lenses in a microscope, we intend to focus light to a geometrical point with less aberration so that the imaging resolution could be improved. Alternatively, the technique of gradient index (GRIN) optics has been applied to design lenses by shaping the spatial distribution of the refractive index of a material rather than the interface of lenses. The resulting lenses can be flat and avoid the typical aberrations of traditional lenses.

[a]*NSF Nanoscale Science and Engineering Center (NSEC), 3112 Etcheverry Hall, University of California, Berkeley, CA 94720, USA. E-mail: xiang@berkeley.edu*
[b]*Materials Science Division, Lawrence Berkeley National Laboratory, 1 Cyclotron Road, Berkeley, CA 94720, USA*

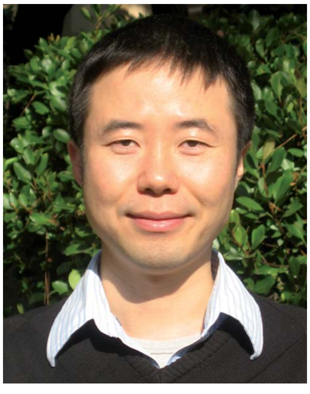

Yongmin Liu

Yongmin Liu received his Ph.D. degree from the University of California, Berkeley in 2009, under the supervision of Prof. Xiang Zhang. Currently he is a postdoctoral researcher in the same group. Dr. Liu will join the faculty of Northeastern University in August 2012, with a joint appointment in the departments of Electrical & Computer Engineering and Mechanical & Industrial Engineering. Dr. Liu's research interests include nanoscale materials and engineering, nano photonics, nano devices, and nonlinear and quantum optics of metallic nanostructures.

Xiang Zhang

Xiang Zhang received his Ph.D. degree from the University of California, Berkeley in 1996. He is Ernest S. Kuh Endowed Chair Professor at UC Berkeley and the Director of NSF Nano-scale Science and Engineering Center. He is also a Faculty Scientist at Lawrence Berkeley National Laboratory. Prof. Zhang is an elected member of National Academy of Engineering (NAE) and Fellow of four scientific societies: American Association for the Advancement of Science (AAAS), American Physical Society (APS), Optical Society of America (OSA), and the International Society of Optical Engineering (SPIE). His research interests are nano-scale science and technology, materials physics, photonics and bio-technologies.

In fact, it has been long known that a spatially changing refractive index modifies light propagation characteristics. Based on the early work of the ancient Greek mathematician Hero of Alexandria (10–70 AD) and the Arab scientist Ibn al-Haytham (965–1040 AD), Pierre de Fermat formulated the famous Fermat's principle to determine how light propagates in materials.[1] This principle states that light follows the extremal optical paths (shortest or longest, although mostly shortest), where the optical path is measured in terms of the refractive index n integrated along the light trajectory. If we replace one material with another one with a different refractive index in the space where light propagates, the light path will be bent or even curved instead of a straight line. Many optical phenomena, such as refraction of a straw at the interface of air and water, and the mirage effect in a desert due to the air density (refractive index) variation, can be explained by Fermat's principle.

Fermat's principle tells us how light propagates, if we know the distribution of the refractive index in space. The emerging field of transformation optics enables us to solve the inverse problem, that is, how to realize a specific light path by designing the variation of material properties.[2–4] Apparently, this is one significant step moving forward. With transformation optics, we have the most general and powerful method to realize almost all kinds of novel optical effects and devices, some of which only existed in science fiction and myths. Tremendous progress has been achieved in the field of transformation optics during the past a few years, thanks to the new electromagnetic theory and modelling software, state-of-the-art fabrication tools as well as greatly improved characterization and analysis techniques. In this review article, we will first outline the general theory of transformation optics and metamaterials that allow for the realization of transformation optical designs. Then we will focus on the most recent advances, both theory and experiment, in transformation optics at optical frequencies and at the nanoscale. Finally, the perspective of transformation optics will be presented.

2. Theory of transformation optics

The fundamental of transformation optics arises from the fact that Maxwell's equations, the governing equations for all electromagnetic effects, are form invariant under coordinate transformations. Assuming no free current densities, in a Cartesian coordinate system Maxwell's equations can be written as

$$\begin{cases} \nabla \times E = -\mu \cdot \partial H/\partial t \\ \nabla \times H = \varepsilon \cdot \partial E/\partial t \end{cases} \quad (1)$$

where E (H) is the electric (magnetic) field, and ε (μ) is the electric permittivity (magnetic permeability) of a medium that can be a tensor in general. It can be rigorously proved that after applying a coordinate transformation $x' = x'(x)$, Maxwell's equations maintain the same format in the transformed coordinate system,[2–4] that is,

$$\begin{cases} \nabla' \times E' = -\mu' \cdot \partial H'/\partial t \\ \nabla' \times H' = \varepsilon' \cdot \partial E'/\partial t \end{cases} \quad (2)$$

In eqn (2), the new permittivity tensor ε' and permeability tensor μ' in the transformed coordinate system are related to the original ε and μ given by[5,6]

$$\begin{cases} \varepsilon' = \dfrac{\Lambda \varepsilon \Lambda^{\mathrm{T}}}{\det|\Lambda|} \\ \mu' = \dfrac{\Lambda \mu \Lambda^{\mathrm{T}}}{\det|\Lambda|} \end{cases} \quad (3)$$

where Λ is the Jacobian matrix with components defined as $\Lambda_{ij} = \partial x'_i/\partial x_j$. The Jacobian matrix characterizes the geometrical variation in the original space x and the transformed space x'. The corresponding electromagnetic fields in the new coordinate are given by

$$\begin{cases} E' = \left(\Lambda^{\mathrm{T}}\right)^{-1} E \\ H' = \left(\Lambda^{\mathrm{T}}\right)^{-1} H \end{cases} \quad (4)$$

Eqn (1)–(4) form the basis of transformation optics. We can design and manipulate the light trajectory by an arbitrary coordinate transformation. Consequently, the material properties and field components need to be rescaled according to the form invariance of Maxwell's equations. This guarantees the physical characteristic of light propagation to be preserved at different scales. In fact, such a correspondence between coordinate transformations and materials parameters has been noticed for a long time.

Probably the most remarkable transformation optical device is the invisibility cloak, which can render an object unperceivable although the object physically exists. One seminal design of such a cloak was proposed by Sir John Pendry *et al.*[2] They considered the hidden object to be a sphere of radius R_1 and the cloaking region to be contained within the annulus $R_1 \le r \le R_2$. By applying a very simple coordinate transformation

$$\begin{cases} r' = R_1 + r(R_2 - R_1)/R_2 \\ \theta' = \theta \\ \phi' = \phi \end{cases} \quad (5)$$

the initial uniform light rays in the central region ($0 \le r \le R_2$) are squeezed into a shell ($R_1 \le r' \le R_2$), while the rest of the light rays (in the region $r > R_2$) are maintained. Waves cannot penetrate into and hence interact with the core region ($0 \le r' \le R_1$), because it is not part of the transformed space. No matter what object is placed inside the core, it appears to an observer that nothing exists; that is, the object is concealed or cloaked. Based on eqn (3), we can calculate the required material properties for the cloaking device. In the region of $r' \le R_1$, ε' and μ' can take any values and do not cause any scattering. In the region of $R_1 \le r' \le R_2$,

$$\begin{cases} \varepsilon'_{r'} = \mu'_{r'} = \dfrac{R_2}{R_2 - R_1}\left(\dfrac{r' - R_1}{r'}\right)^2 \\ \varepsilon'_{\theta'} = \mu'_{\theta'} = \dfrac{R_2}{R_2 - R_1} \\ \varepsilon'_{\phi'} = \mu'_{\phi'} = \dfrac{R_2}{R_2 - R_1} \end{cases} \quad (6)$$

Finally, for $r' \ge R_2$ the properties of materials are unchanged.

Under the short wavelength limit ($R_1, R_2 \gg \lambda$), the ray tracing results confirm the performance of the invisibility cloak as shown in Fig. 1(a). The rays, which represent the Poynting vector or energy flow, are numerically obtained by integration of a set of Hamilton's equations taking into account the anisotropic,

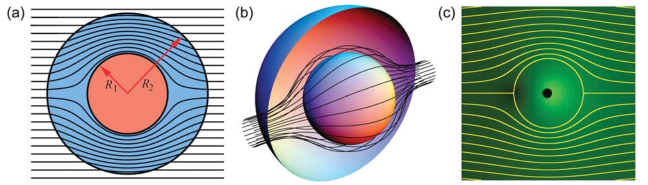

Fig. 1 (a) A schematic of a cloak in a two-dimensional view, reprinted from ref. 2 with permission. The rays, representing the Poynting vector, divert within the annulus of the cloak region ($R_1 < r < R_2$), while emerging on the far side without any scattering and distortion. (b) Ray tracing results for an invisibility cloak in a three-dimensional view, reprinted from ref. 2 with permission. (c) Ray propagation in the dielectric invisibility device, reprinted from ref. 8 with permission. The light rays (shown in yellow) smoothly flow around the interior cloak region (shown in black). The brightness of the green background indicates the refractive index profile taken from the Kepler profile.

inhomogeneous material properties in the compressed region ($R_1 \le r' \le R_2$).[2,6] Light is smoothly wrapped around the core, and the propagation characteristic is preserved outside the cloak. This implies that any object placed in the interior region appears to be concealed, since there is no diffracted or scattered light in the presence of the object. Full-wave simulations without geometric optics approximation also verify the cloaking effect.[7]

It is worth mentioning that different approaches have been proposed to realize invisibility cloaks. One example is the conformal mapping technique to design the refractive index profile that guides light around an object.[8,9] We can introduce a new coordinate w described by an analytic function $w(z)$ that does not depend on z^*, where a complex number $z = x + i \times y$ is used to describe the spatial coordinate in a two-dimensional (2D) plane and z^* stands for the conjugate of z. Such a function defines a conformal mapping that preserves the angles between the coordinate lines. For a gradually varying refractive index profile, both the electric and magnetic fields satisfy the Helmholtz equation. In the new coordinate w, the Helmholtz equation has the same format with a transformed refractive index profile that is related to the original one as $n' = n \cdot \left|\frac{\mathrm{d}w}{\mathrm{d}z}\right|^{-1}$. By interpreting the Helmholtz equation in the coordinates w as the Schrödinger equation of a quantum particle in the Kepler potential, Leonhardt designs a dielectric invisibility cloak with refractive index ranging from 0 to about 36 (Fig. 1(c)). Different from the transformation optics approach, the conformal mapping technique is strictly two-dimensional. However, the conformal mapping idea can be extended to non-Euclidean geometry to realize three-dimensional (3D) cloaks, and eliminate the extreme values of materials parameters that often appear in the method of transformation optics.[10] The conformal mapping method has been used for designing a variety of devices in addition to the invisibility cloak.[11–15] Moreover, it has been shown that conformal mapping performs well even in the regime beyond geometrical optics.[16] Another type of approximate invisibility cloaking is a core–shell structure. It has been shown that a negative-permittivity shell can significantly reduce the scattering cross-section of a small positive-permittivity core in the quasi-static limit.[17,18] By exploiting the frequency dispersion of metals and their inherent negative polarizability, it is shown that covering a dielectric or conducting object of a certain size with multilayered metallic shells may reduce the "visibility" of the object by several orders of magnitude simultaneously at multiple frequencies.[19] Meanwhile, researchers have been actively exploring the interesting physics associated with invisibility cloaks,[20–24] or trying to detect an invisibility cloak.[25,26]

The invisibility cloak has triggered widespread interest in transformation optics. Many other novel effects and devices, such as illusion optics,[27–30] optical black holes,[31–34] beam shifters and rotators,[35–37] lossless waveguide bends[38–41] as well as various lenses[42–50] have been proposed. In particular, combining the concept of complementary medium[51] with transformation optics, Yang *et al.* proposed a superscatter which can enhance the electromagnetic wave scattering cross section, so that it appears as a scatter with a larger dimension.[52] Subsequently, Chan's group theoretically conceived and numerically demonstrated a general concept of illusion optics: making an arbitrary object appear like another object with a completely different shape and material constituent.[27] Cloaking can be considered as the creation of an illusion in free space. The principle behind illusion optics is not light bending but rather the cancellation and restoration of the optical path of light by using negative-index materials. The key of an illusion device lies in two distinct pieces of materials, that is, a complementary medium and a restoring medium. The complementary medium annihilates the adjacent space and cancels any light scattering from an object itself. Then the restoring medium recovers the cancelled space with a new illusion space that embraces another object chosen for the illusion. Numerical simulations confirm the performance of the illusion device, which transforms the field distribution scattered from a dielectric spoon into the scattering pattern from a metallic cup. More interestingly, the illusion device can work at a distance from the object. It is shown that this "remote" feature enables the opening of a virtual aperture in a wall so that one can peep through the wall. Lai *et al.* also numerically demonstrate a remote invisibility cloak that can cloak an object at a certain distance outside the cloaking shell rather than encircled by the cloaking shell.[53] Unlike previous light-bending cloaking devices,[2–9] the constitutive parameters of illusion devices do not need a complex spatial distribution. However, materials with a negative refractive index are required in the design, which are not obtainable in nature.

3. Metamaterials for realizing transformation optical designs

Although transformation optics provides the most general means to design exotic optical effects and elements, the experimental realization of them is far from trivial. As shown in eqn (3), both electric permittivity and magnetic permeability need to be spatially and independently tailored. Moreover, the resulting material properties are anisotropic in general, and may require unusual values (negative, zero or infinity). We are limited in natural materials to fulfil such demands. For example, natural materials only show magnetism ($\mu/\mu_0 \neq 1$) up to terahertz frequencies. Fortunately, the emerging field of metamaterials offers an entirely new route to design material properties at will, so that the transformation optical design could be experimentally realized.[54–61] Different from natural materials, the physical properties of metamaterials are not primarily dependent on the chemical constituents, but rather on the internal, specific structures of the building blocks of metamaterials. These building blocks function as artificial "atoms" and "molecules", in analogy to those in natural materials. Through regulated interactions with electromagnetic waves, they can produce extraordinary properties that are difficult or impossible to find in naturally occurring or chemically synthesized materials.

Metamaterials consist of periodically or randomly distributed artificial structures, whose size and spacing are much smaller than the wavelength of electromagnetic waves. As a result, the microscopic detail of individual structures cannot be sensed by electromagnetic waves. What matters is the average result of the collective response of the whole assembly. In other words, we can homogenize such a collection of inhomogeneous objects and define effective material properties at the macroscopic level. This is effective media approximation, which has been well known.[62] The most attractive aspect of metamaterials, however, is that the material properties can be controlled by properly engineering the structures. For instance, metallic wire arrays[63] and metallic split-ring structures[64] can produce effective ε and μ, respectively, with tunable values ranging from positive to negative within a certain wavelength range. By combining the two basic structures with simultaneously negative ε and μ, we can even create materials possessing a negative refractive index that enable negative refraction[65–69] and perfect imaging.[70–74] Furthermore, metamaterials allow us to achieve unusual anisotropy[75–77] and chirality.[78–80] We refer readers to recent review papers and books for more insights in the field of metamaterials.[54–61]

The complete control over electric permittivity and magnetic permeability offered by metamaterials turns transformation optical design into reality. In 2006, Smith's group demonstrated the first invisibility cloak in the microwave region.[81] To mitigate the fabrication and measurement challenges, a 2D cylindrical cloak instead of a 3D spherical one was implemented. Since the electric field is polarized along the z axis of the cylindrical coordinate, in the transformed ε' and μ' tensors only ε_z', μ_r' and μ_θ' are relevant. After a further renormalization, the reduced material parameters are

$$\varepsilon_z' = \left(\frac{R_2}{R_2 - R_1}\right)^2, \mu_r' = \left(\frac{r' - R_2}{r'}\right)^2, \mu_\theta' = 1 \qquad (7)$$

where the interior and exterior radium of the cloaking device is R_1 and R_2, respectively. The advantage of using reduced material properties is that only one parameter (μ_r') spatially varies while the other two are constant throughout the structure. This parameter set is realized in a metamaterial structure consisting of split-ring resonators with carefully designed geometries (Fig. 2(a)). In the experiment, a field-sensing antenna is used to record the field amplitude and phase inside the cloak and in the surrounding free-space region. The experimental results show that the cloak can significantly decrease scattering from the hidden object and also reduce its shadow. From Fig. 2(b) and (c), one can clearly see that electromagnetic waves smoothly flow around the cloak, and propagate to the far side with only a slightly perturbed phase front, which is mainly due to the reduced parameter implementation. In comparison, a bare Cu cylinder without the cloak produces much stronger scattering in both the forward and backward directions.

4. Broadband transformation optical design at optical wavelengths

The pioneering work on transformation optics in 2006 (ref. 2, 3 and 6) stimulated the global attention of researchers in different disciplines. Ever since then, tremendous effort has been devoted to the field of transformation optics. Considering the great application potential, one prime direction of transformation optics is to implement designs working in the optical regime.[82] However, most transformation optical devices rely on metamaterials, in which the building blocks are normally much smaller than the wavelength of interest. This indicates that the feature size of the device should be precisely controlled at the scale of a few hundred or even below one hundred nanometers. More importantly, metamaterials are usually resonant structures with narrow operation bandwidth and high loss. These two factors impose severe challenges on the implementation of transformation optical devices with broad bandwidth and low loss at near-infrared and visible frequencies. New designs and creative fabrication techniques are imperative to tackle the challenges.

In the following, we will concentrate on the discussion of the carpet cloak introduced by Jensen Li and John Pendry,[83] although other designs, such as one-dimensional (1D) cloaks[84,85]

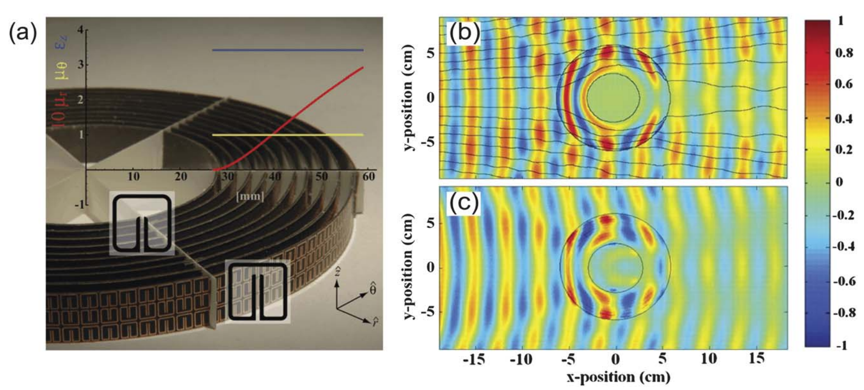

Fig. 2 (a) An image of a 2D microwave cloak made of split-ring resonators. The background plots the values of the prescribed material properties for the cloak. The split-ring resonator of layer 1 (inner) and layer 10 (outer) are shown in the transparent square insets. (b) Simulated and (c) experimentally mapped field patterns of the cloak. Reprinted from ref. 81 with permission.

and cloaks using non-Euclidean geometries,[10] can also operate over a relatively wide range of wavelengths. Different from the original complete cloak that essentially crushes the object to a point and works for arbitrary incident angles, the carpet cloak crushes the object to a sheet and the incident angle is limited within the half space of a 2D plane. However, the carpet cloak does not require extreme values for the transformed material properties. Moreover, by applying the quasi-conformal mapping technique, the anisotropy of the cloak can be significantly minimized. Consequently, only isotropic dielectrics are needed to construct the carpet cloak (Fig. 3(a)), implying the device could be broadband and practically scalable to operate in the optical regime. Full-wave simulations confirm that the carpet cloak successfully imitates a flat reflecting surface. As shown in Fig. 3(b), the light reflected from a curved reflecting surface, on top of which is covered with the carpet cloak, well maintains the flat wavefront without any distortion. It seems that the light is reflected by a flat ground plane. Therefore, it renders an object placed underneath the curved bump invisible. In contrast, if the cloak is absent, the incident beam is deflected and split into two different angles (Fig. 3(c)).

Soon after the demonstration of a microwave carpet cloak based on non-resonant metallic metamaterials,[86] three groups independently realized the carpet cloak in the near-infrared region.[87–89] Interestingly, all of them utilized the same dielectric platform (silicon-on-insulator (SOI) wafer) to achieve the broadband and low-loss carpet cloak, although the configurations are different. In the design of Zhang's group,[87] the carpet cloaking device consists of two parts (Fig. 4(a) and (b)): a triangular region with a uniform hole pattern that acts as a background medium with a constant effective index (1.58), and a rectangular region with varying hole densities to realize the spatial index profile similar to Fig. 3(a). The holes with a constant diameter (110 nm) were made through the Si layer by focused ion beam (FIB) milling. Under the effective medium approximation, the desired spatial index profile can be achieved by controlling the density of holes through the relation $\varepsilon_{\rm eff} = \varepsilon_{\rm air}\,\rho_{\rm air} + \varepsilon_{\rm Si}\,\rho_{\rm Si}$, where ρ is the volumetric fraction and ε is the effective dielectric constant of each medium. In addition, two gratings were fabricated in order to couple light into and out of the Si slab waveguide. Finally, directional deposition of 100 nm gold was carried out using electron beam evaporation to create the reflecting surface. In the experiments, the authors characterize the reflected beam profile of a Gaussian beam in three scenarios: (1) a flat surface without a cloak, (2) a curved surface with a cloak and (3) a curved surface without a cloak. It is observed that in both case (1) and (2), the reflected beam preserves the Gaussian profile, similar to the incident waves. In a sharp contrast, the light

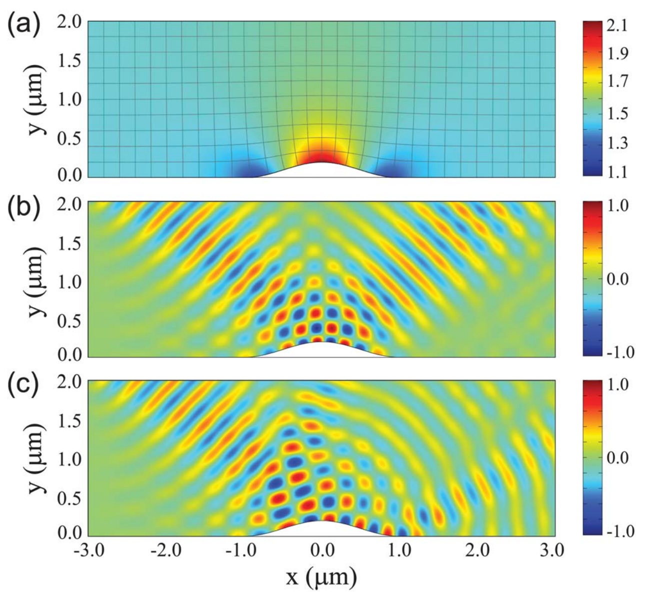

Fig. 3 (a) The colour maps show the transformed material properties (refractive index n). The grey lines represent the transformed grid after the quasi-conformal mapping. All of the square cells in the original Cartesian coordinate are transformed to nearly squares of a constant aspect ratio after the quasi-conformal mapping. Consequently, the anisotropy of the material property is minimized to a negligible degree. Comparing with the background (SiO_2 with n = 1.45), the resulting refractive index is higher in the region above the curved bump, while it is lower at the two shoulders of the bump. (b) The electric field pattern for a Gaussian beam launched at 45° towards the ground plane from the left, with the spatial index distribution given in (a). (c) The electric field pattern when only the curved bump is present without the cloak. The wavelength is 500 nm for simulation in (b) and (c).

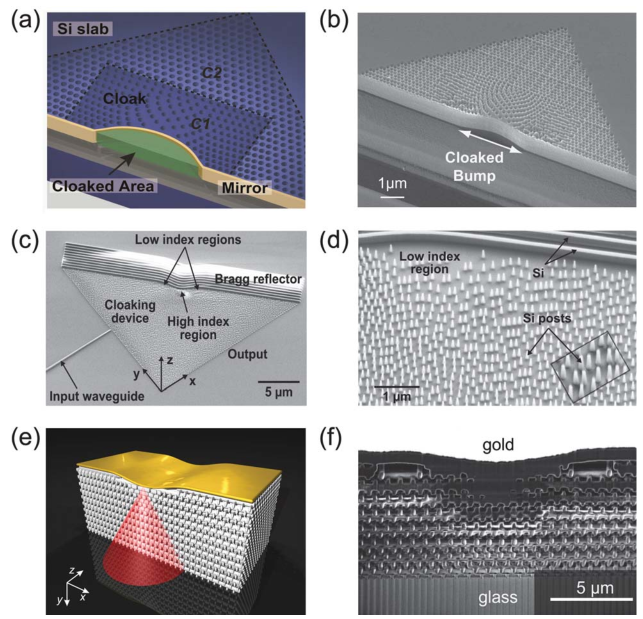

Fig. 4 (a) Schematic and (b) scanning electron microscope (SEM) image of a near-infrared carpet cloak, which is realized by milling holes with different densities in a SOI wafer. Reprinted from ref. 87 with permission. In the schematic figure (a), the rectangular cloak region marked as C_1 has a varying index profile given by the transformation design, and the triangular region marked as C_2 has a uniform hole pattern, serving as a background medium with a constant effective index of 1.58. (c) and (d) SEM images of another near-infrared cloaking device by etching silicon posts in a SOI wafer. Light is coupled into the device *via* an input waveguide and reflected by the Bragg mirror towards the x–z plane. Reprinted from ref. 88 with permission. (e) Schematic and (f) cross-sectional SEM image of a 3D carpet-cloak structure working in the near-infrared region, reprinted from ref. 90 with permission. The 3D cone of light in (e) corresponds to the NA = 0.5 microscope lens.

reflected from the uncloaked bump (case (3)) shows three distinct spots at the output grating due to the scattering of the bump. These results unambiguously verify the performance of the carpet cloak. Furthermore, since the device is composed of dielectric materials rather on resonant elements, it is expected to operate over broad wavelengths. Indeed, for wavelengths ranging from 1400 to 1800 nm, the reflected beam from the cloaked curve surface shows a single peak at the output grating.

In comparison, the carpet cloak demonstrated by Lipson's group is a complementary structure.[88] Instead of milling holes in the SOI wafer, they etched silicon posts of subwavelength 50 nm in diameter with spatially varying density and cladded the device with SiO_2 medium (Fig. 4(c) and (d)). In addition, the reflective surface is composed of a dielectric distributed Bragg reflector (DBR) with a deformation that covers the cloaked region rather than a metallic film. It is experimentally observed that the output of the light propagating through the cloak and incident on the curved DBR mirror resembles the image from a flat mirror without any distortion. In another similar work, light propagation inside a silicon-nanorod-based carpet cloak is imaged by near-field scanning optical microscopy (NSOM), providing a direct visualization of the cloaking effect.[89]

The aforementioned work represents a major step towards general transformation optics at optical frequencies. They also show potentials to realize a variety of transformation optical devices in on-chip silicon photonic footprints. However, the demonstrated carpet cloaks were essentially based on a 2D waveguide configuration, implying that the cloaking effect only works in the plane. In other words, the devices are visible in the third dimension. Tolga Egin and his colleagues extrude the third dimension of the original carpet cloak design, rendering the cloaking to work in a 3D setting for reasonably large viewing angles (Fig. 4(e)).[90] They implement a design based on tailored, dielectric face-centered-cubic (FCC) wood-file photonic crystals. The diamond-symmetry woodpile geometry is chosen for its nearly isotropic optical properties. The technique of direct laser writing *via* multiphoton polymerization of a negative photoresist was used to fabricate the 3D photonic crystals. By properly controlling the position and intensity of the writing laser beam, an arbitrary three-dimensional connected pattern, either periodic or non-periodic, can be created. Fig. 4(f) shows the interior of the fabricated carpet cloak after FIB milling. The background is a homogeneous woodpile structure. Within the cloak region, the local effective refractive index is controlled by the volume filling ratio of the polymer and air void. In the optical measurement, the samples are illuminated by unpolarized light from an incandescent lamp. The carpet plane is imagined through the glass substrate on an image plane. A single reflective Cassegrain lens with numerical aperture NA = 0.5 is used to avoid chromatic aberrations. This NA corresponds to a 3D illumination and full viewing angle of about 60°. A multimode optical fibre is scanned across the image plane in order to measure the spatial and spectral dependence. The light emerging from the other end of the fibre is collimated and sent into a home-made Fourier transform spectrometer. In both bright-field and dark-field optical spectroscopy measurements, it is observed that scattered light from the cloaking device is drastically suppressed over a broad wavelength spectrum (1.5–2.6 μm) in comparison with the uncloaked bump, which is consistent with ray-tracing calculations.[91] Interestingly, this result implies that the effective medium approximation may even work as approaching the Wood anomaly wavelength, since the lattice constant (0.8 μm) of the photonic crystals is already comparable with the operation wavelength. It is theoretically shown that transformation optical devices can be achieved in the photonic crystal platform, by either searching different types of constant frequency contours to approximate a specific effective medium profile or manipulating Bloch waves in curved and gradient photonic crystals.[92–94]

Recently, Fischer *et al.* reduced the lattice constant of the previous photonic crystal structure by a factor of more than 2, and successfully realized a 3D carpet cloak for unpolarized light at visible wavelengths.[95] Inspired by stimulated-emission-depletion (STED) fluorescence microscopy, the authors significantly improved the lithography resolution of direct laser writing.[96] By overlapping a femtosecond excitation beam spot and a continuous-wave depletion beam, the effective exposure volume for the photoresist (0.25 wt% 7-diethylamino-3-thenoylcoumarin in pentaerythritol tetraacrylate) can be greatly reduced. Consequently, the lithography resolution could overcome the diffraction-limit. Fig. 5(b) shows SEM images of the cross-section of the homogeneous woodpile photonic crystal (the reference sample)

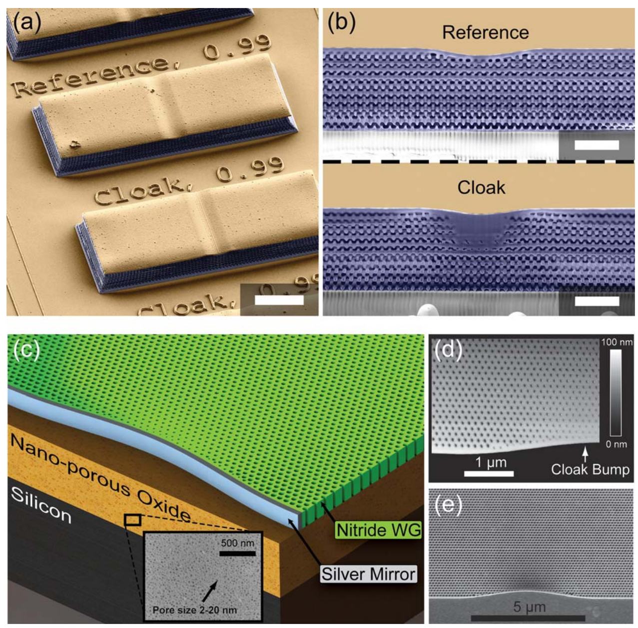

Fig. 5 (a) A false-coloured SEM image of the polymer reference (top) and 3D carpet cloak (bottom) structures working at visible wavelengths, which are fabricated on a glass substrate and coated with 100 nm gold. The scale bar corresponds to 10 μm. (b) SEM images showing the cross-section of the reference and cloak after FIB cut. The scale bar corresponds to 2 μm. (a) and (b) are reprinted from ref. 95 with permission. (c) A schematic of the cloak device implemented in a SiN waveguide on a low index nanoporous silicon oxide substrate. The SiN layer and the nanoporous oxide layer are 300 nm and 5–10 μm thick, respectively. The diameter of holes varies in size from 65 to 20 nm. The inset shows an SEM image of the low-index nanoporous silicon oxide substrate. (d) An atomic force microscope (AFM) image of the hole pattern as transferred to the electron beam resist after development. (e) An SEM image of the fabricated carpet cloak device, consisting of roughly 3000 holes. (c)–(e) are reprinted from ref. 98 with permission.

as well as of the carpet cloak device. The lattice constant of the photonic crystal is 350 nm. Reflection optical measurements at different visible wavelengths and incident angles, along with the interferometric phase measurement[97] strongly confirm the 3D polarization-independent cloaking effect in the visible region.

A carpet cloak in the waveguide geometry for visible light has also been demonstrated,[98] with two important modifications compared with the Si carpet cloak working at the near-infrared frequency.[87] First, a silicon nitride (SiN) slab is used as the footprint, since silicon becomes lossy due to absorption at visible wavelengths. Second, nanoporous silicon oxide with very low index ($n < 1.25$) is developed for the substrate, which increases the available index modulation and enables the realization of transformation optics for guided visible light in the SiN slab. By repeating electrochemical etching and oxidation, a solid silicon layer is slowly consumed, leaving solid filling fractions as low as 15%. Once the desired porosity is reached, the entire silicon network is converted to a porous silicon oxide medium by oxidizing at high temperature (800 °C). The pore size ranges from 2 to 20 nm (shown in the inset of Fig. 5(c)), and the surface roughness is less than 3 nm rms. A 300 nm SiN slab waveguide is deposited on the low index substrate using plasma-enhanced chemical vapour deposition (PECVD). Finally, a two-step pattern transfer process is applied to fabricate the hole pattern with a fixed hexagonal lattice constant (130 nm) but varied hole sizes (20–65 nm). In the optical measurement scheme similar to ref. 87, it is shown that at three different wavelengths (480, 520, and 700 nm), the reflection from the uncloaked bump produces a clear perturbation in the wavefront in comparison with the reflection from a flat mirror. The cloaking device, on the other hand, reconstructs the wavefront and results in a beam profile identical to the original Gaussian beam reflected from a flat mirror. This confirms that the designed transformation effectively cloaks the uneven surface throughout the entire visible spectrum. The platform based on the SiN slab and low-index porous silicon oxide substrate leads to a general implementation of optical transformation structures in the visible range.

The aforementioned carpet cloaks in the planar Si or SiN geometry can be readily extended to other transformation optical designs. In particular, it is feasible and desirable to combine transformation optics with on-chip photonics for much broader functionalities.[99–102] Traditional integrated photonics collects individual, discrete optical elements, such as the light source, waveguide, modulator, detector, *etc.* on a footprint. Employing the transformation optics method, Zentgraf *et al.* have successfully designed and demonstrated a photonic "Janus" device which simultaneously possesses multiple functions within one single optical element.[99] This opens up a new avenue to achieving a high density of functionalities, effectively scaling down the size of integrated photonic circuits. As shown in Fig. 6(a), we can combine a lens and a beam-shifter into the same device, while working along the horizontal and vertical direction, respectively. The theoretically designed permittivity profile of the "Janus" device is translated into a pattern of 75 nm air holes with a spatially varying density (inset of Fig. 6(a)). In the optical measurements, the excitation of the slab TM waveguide mode, which passes the lens along the horizontal direction, is performed using a Gaussian beam with a spot diameter of 13 μm at the input grating, while a small beam spot with a diameter of 2 μm is used for the beam-shifter in the vertical direction. From Fig. 6(b), one can see that the large beam spot is strongly reduced after passing the "Janus" device along the x-axis. In contrast, if the beam is propagating through the device along the y-axis, it is shifted at the output grating from left to right and *vice versa* (Fig. 6(c)). The measurement of the device shows that the element works over a range of 100 nm for a center wavelength of 1.5 μm.

5. Macroscopic transformation optical devices

One ultimate goal of transformation optics is to realize practical devices at the macroscopic level. For instance, we want to hide realistic, large objects using invisibility cloaks. The demonstrated cloaks at microwave and terahertz frequencies are physically large, and range from centimetres to millimetres.[81,86,103–105] In other words, they are in the order of around 100 wavelengths or less. However, how to observe the cloaking effect with naked eye, *i.e.*, to cloak a macroscopic object in the visible regime was thought extremely challenging. As we have discussed, almost all transformation optical design operating at visible wavelengths are fabricated by state-of-the-art micro-/nano-manufacturing techniques, including electron-beam lithography, FIB milling and direct laser writing, in order to realize the spatially complex material properties. If we rely on these top-down methods, it is very difficult and time-consuming to realize macroscopic transformation optical devices for visible light, because we need to precisely control the feature size at the nanoscale over a large domain that may be 1000 times larger than the operation wavelength in all three dimensions.

In early 2011, two groups independently reported the demonstration of a macroscopic volumetric cloaking device

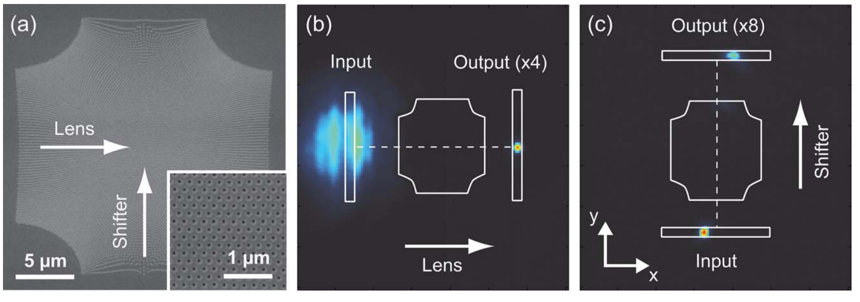

Fig. 6 A photonic "Janus" device for integrated photonics, reprinted from ref. 99 with permission. (a) SEM images of the device consisting of a lens and a beam-shifter. The inset shows a magnified view of the air holes in the silicon waveguide slab. (b) and (c) represent the optical microscope images with the intensity distribution at the in-couple and out-couple gratings for the lens and the shifter, respectively.

based on a very similar design and optical characterization scheme.[106,107] The cloaking design uses calcite, a natural birefringent crystal, thus eliminating time-consuming nanomanufacturing processes and enabling one to hide objects at the scale of millimetres. The demonstrated cloaking device can be still regarded as a carpet cloak. However, it is achieved with spatially homogeneous, anisotropic dielectric materials, in contrast to the original proposed one with inhomogeneous, isotropic material properties. Furthermore, it has been pointed out that the original carpet cloak based on the quasi-conformal mapping method generally gives rise to a lateral shift of the scattered wave, which may make the object detectable.[108]

Fig. 7(a) shows an illustration of the carpet cloak design in ref. 106. A triangular cross-section (blue) in a virtual space is mapped to a quadrilateral region (brown). A small triangular region (grey) is opened up wherein objects can be placed and rendered invisible. The transformation can be mathematically described by

$$x' = x, \quad y' = \frac{H_2 - H_1}{H_2}\cdot y + \frac{d - x\cdot \mathrm{sgn}(x)}{d}\cdot H_1, \quad z' = z \qquad (8)$$

where (x, y, z) and (x', y', z') correspond to the coordinates of the virtual space and physical space, respectively. Following eqn (3) and assuming that the virtual space is filled with an isotropic material property of ε and μ ($\mu = 1$), it is straightforward to obtain reduced material properties of the quadrilateral cloaking region for transverse-magnetic (TM) polarized light propagating in the x–y plane,

$$\varepsilon'_{x-y} = \varepsilon \begin{pmatrix} \left(\frac{H_2}{H_2 - H_1}\right)^2 & -\frac{H_1 H_2^2}{(H_2 - H_1)^2 d}\mathrm{sgn}(x) \\ -\frac{H_1 H_2^2}{(H_2 - H_1)^2 d}\mathrm{sgn}(x) & 1 + \left(\frac{H_2}{H_2 - H_1}\right)^2 \left(\frac{H_1}{d}\right)^2 \end{pmatrix}$$
$$\mu'_z = 1 \qquad (9)$$

Here, ε'_{x-y} is the permittivity tensor in the x–y plane and μ'_z is the permeability element along the z-axis after the transformation. Eqn (9) indicates that such a triangular cloak only requires spatially invariant, anisotropic materials, such as calcite and calomel, which are readily available in macroscopic sizes.

The macroscopic carpet cloak of ref. 106 is realized by gluing two calcite prisms together with the protruding bottom surface of the cloak serving as a deformed reflecting mirror (Fig. 7(b)). Calcite is a uniaxial birefringent crystal whose refractive indices are about 1.66 and 1.49 for ordinary and extraordinary light, respectively, at the wavelength of 590 nm. To meet the material requirement give by eqn (9), the optical axis orientation angle with respect to the y-axis, as well as other geometrical parameters, need to be carefully designed. The cloak region has a triangular cross-section formed by the two bottom facets, and the height of the triangle is close to 1.2 mm, which is more than three orders of magnitude larger than the visible wavelength.

To directly visualize the cloaking effect, a mask with an arrow pattern is placed in front of a green laser (532 nm wavelength), so that the emitted laser beam contains the same pattern (Fig. 7(c)). When light is reflected from the triangular bottom bump, the distortion of the reflected image tells us whether the cloaking effect is achieved or not. In addition, a linear polarizer is used to control the light polarization. The image of the laser beam reflected by a flat mirror is shown in the top panel of Fig. 7(d), which is a horizontally flipped arrow pattern. Since the cloak does not work for TE polarized light, the reflection from the bottom bump splits the laser beam into two (middle panel). In contrast, the reflected beam for TM polarization almost completely conserves the arrow pattern, except for a small dark stripe in the center due to the imperfection in the alignment of the two calcite crystals (bottom panel). Other characterizations, such as different incident angles and white light illuminations, further verify the performance of the cloak.

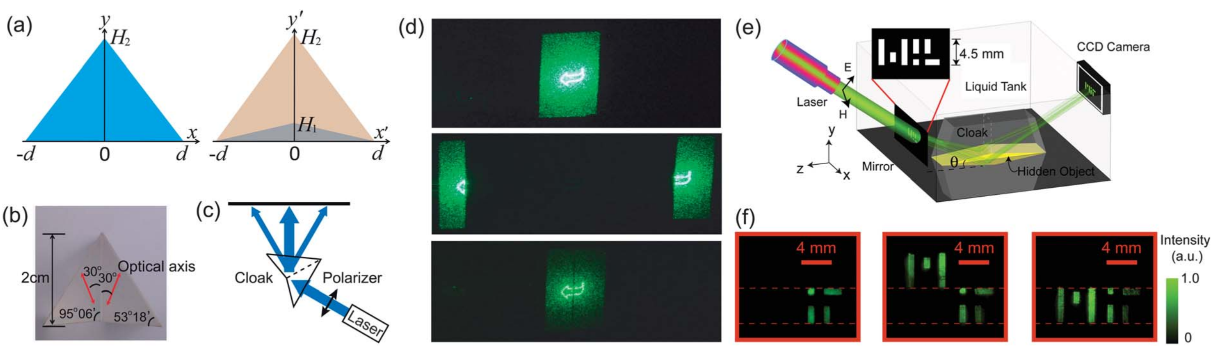

Fig. 7 (a) A schematic of the macroscopic carpet cloak design, in which a triangular cross-section (blue) filled with isotropic materials is mapped to a quadrilateral region (brown) with uniform and anisotropic optical properties. The cloaked region is the small triangle area (grey) wherein objects can be rendered invisible. (b) A photograph of the triangular cloak with the geometrical parameters indicated in the figure. The dimension of the cloak along the z-axis is 2 cm. The optical axis of the calcite crystal, represented by red arrows, is oriented with an angle of 30° relative to the y-axis. (c) A schematic of the experimental setup. The laser goes through a mask with an arrow pattern and then a polarizer. Subsequently, it is reflected by the calcite cloak and projected on a screen. (d) The pattern of the laser beam reflected from a flat mirror, and from the calcite cloak for TE and TM polarizations are shown in the top, middle and bottom panel, respectively. The laser beam reflected by the triangular protruding surface for TM polarization resembles the reflection from a flat surface. (a)–(d) are reprinted from ref. 106 from permission. (e) A schematic diagram of the experimental setup for another calcite carpet cloak designed by the MIT group. (f) Optical images captured on a CCD camera. The three panels from left to right show the reflected images with an uncloaked wedge, a flat mirror on top of the wedge and a cloaked wedge, respectively, at the wavelength of 561 nm. (e) and (f) are reprinted from ref. 107 with permission.

In another work conducted by a research group at MIT,[107] the cloak is designed in a similar approach and also made of two pieces of calcite crystals with specific orientations of the optical axis. The optical characterization scheme also resembles ref. 106. A hollow transmission pattern reading "MIT" is printed on an opaque plastic plate. The pattern is then illuminated by a continuous wave laser with TM polarization. The illumination condition is carefully chosen such that the light transmitted through the inverted "M" goes through the cloak device with the hidden wedge underneath, while the light through the inverted "IT" is directly reflected by the mirror surface. If the cloak works and hides the wedge object successfully, the CCD camera should capture an undistorted "MIT" as if there is nothing on top of the flat mirror. As shown in the sequential panels of Fig. 7(f) from left to right, when light illuminates the wedge only without the cloak placed on top of the mirror, the letter "M" in the reflected laser beam is far away from "IT" and missed in the CCD image. When there is a flat reflecting plane on top of the wedge, the letter "M" is undistorted, but it is shifted upwards compared with "IT". Only for the cloaking device, does the CCD image show the correct "MIT" pattern, as if the cloaked wedge does not exist. Using calcite crystals, a simplified hexagonal cloak which works for six incident directions has been demonstrated very recently.[109] Although these works show the possibility of realizing practical transformation optical devices without suffering complicated micro-/nano-fabrication fabrication processes, the demonstrated cloak is essentially limited in 2D geometry, because light must propagate in one plane and polarize in one direction. It is possible to extend such 2D cloaks into truly 3D geometries working in the visible spectrum.

6. Transformation optics for plasmonics

Transformation optics in principle embraces all forms of electromagnetic phenomena at all length scales. Although most work is devoted to manipulating propagating waves in free space, recently there has been a keen interest in transforming near-field optical waves, such as surface plasmon polaritons (SPPs). Surface plasmon polaritons are collective charge oscillations existing at the interface between a metal and a dielectric.[110] They are driven by and coupled with the electric field of external electromagnetic waves, behaving as propagating or localized optical surface waves at the metal–dielectric interface. Due to the tight confinement and strong field enhancement, SPPs are widely used for various purposes at the subwavelength scale, ranging from nano optical circuitry,[111–114] microscopy,[74,115] lithography,[116,117] and data storage,[118,119] to biosensing[120,121] and photovoltaics.[122] Such a new research paradigm, called plasmonics, has become a very active branch in nano optics. Merging transformation optics with plasmonics is expected to give rise to a host of fascinating near-field optical phenomena and devices.

SPPs are bound surface waves at metal–dielectric interfaces, implying that the entire domain, both the metal and dielectric materials, needs to be transformed if we rigorously follow the transformation optics approach. In practice, it is extremely difficult, if not impossible, to spatially modify the metal property at the deep subwavelength scale. Fortunately, we can overcome this problem *via* prudent designs. For example, as pointed out by Liu *et al.*[123] and Huidobro *et al.*[124] independently, one can control SPPs by solely modifying the dielectric material based on the transformation optics technique, since a significant portion of SPP energy is carried in the dielectric medium at optical frequencies. Moreover, the transformed dielectric materials can be isotropic and nonmagnetic if an advanced transformation technique, such as conformal or quasi-conformal transformation, is performed.

We take the similar geometry of the carpet cloak as an example to show how the propagation characteristic of SPPs can be modified and the scattering of SPPs due to surface topology can be considerably suppressed.[123] Scattering of SPPs exists whenever there is a variation in geometries or material properties.[125] In addition to the intrinsic Ohmic losses of metals, scattering can be a major loss factor that limits the propagation length of SPPs. Fig. 8(a) shows full-wave simulation at 633 nm wavelength, where SPPs at the air–silver interface are launched from the left-hand site and then pass a surface protrusion. One can clearly see that the protrusion gives rise to forward scattering into free space. Quantitatively, about 26% of the SPP energy is radiated to the far field in this scattering process. This is a fairly big loss, considering that the energy attenuation due to the Ohmic loss is only about 4% for SPPs propagating the same lateral distance. In contrast, once we apply the refractive index profile on top of the metal surface following the coordinate transformation to map a

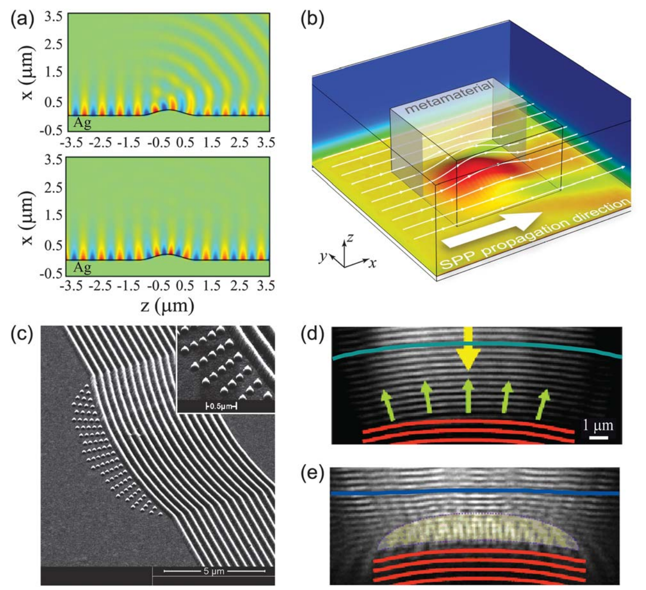

Fig. 8 (a) A 2D transformation plasmonic structure (bottom panel), which can significantly suppress the scattering of SPPs due to the uneven metal surface (top panel). Reprinted from ref. 123 with permission. (b) Power flow distribution (color map) and streamlines of a 3D carpet cloak, reprinted from ref. 124 with permission. (c) An SEM image of the designed plasmonic cloak. The cloak is made of TiO_2 nano-pillars, as shown in the inset. (d) and (e) are leakage radiation images of SPPs for a bare curved Bragg-reflector and a plasmonic cloak, respectively. When the incident SPPs (yellow arrow) hit a curved Bragg mirror (red curves), the back reflected SPPs (green arrows) have different directions due to the curved shape of the reflector. If the cloak (purple dotted line) is placed in front of the curved Bragg mirror, the beating pattern in reflection has an almost flat wavefront, similar to the reflection from a straight Bragg reflector. (c)–(e) are reprinted from ref. 126 with permission.

protruded surface to flat one, the scattering of SPPs is almost completely eliminated. The surface appears virtually flat for the SPPs, although physically the surface protrusion exists. Since solely isotropic and nondispersive materials are used to realize the transformed dielectric material, one major advantage of the transformation plasmonic structure is the broadband performance. For wavelengths from 850 to 450 nm, scattering loss increases from 14% to 43% before the transformation. After the transformed dielectric cladding is applied, strikingly, the scattering loss of the SPPs is below 4.5% over the entire wavelength region. A 3D carpet cloak designed from transfinite mapping can also work effectively for bounding SPPs at the uneven metal surface, although in this case the transformed material is anisotropic.[124] The color map and the streamlines in Fig. 8(b) represent the density and the direction of the power flow of SPPs, respectively. SPPs are guided around the bump and continue traveling along the air–gold interface with only slight scattering.

Almost at the same time of the publication of ref. 123 and 124, Quidant's group experimentally demonstrated the plasmonic carpet cloak.[126] The configuration is shown in Fig. 8(c), where a gold surface is structured with TiO_2 nano-pillar structures to realize the required refractive index profile. A curved Bragg-type reflector, consisting of 15 gold lines periodically separated by half of the SPP wavelength, is employed to act as the object to be hidden behind the carpet. Leakage radiation microscopy (LRM) images map the distribution of the SPPs propagating at the air–gold interface. In the case of a bare curved Bragg-reflector, the reflected SPPs are propagating into different directions depending on their relative angles to the normal of the mirror lines, leading to a curved wave front (Fig. 8(d)). Conversely, incorporating TiO_2 nano-pillar structures recovers a fringe pattern in the reflected SPPs with a nearly straight wave front, similar to the reflection from a flat Bragg-mirror (Fig. 8(e)). The remaining small lateral modulations are attributed to imperfections in the manufacturing. Data analysis further quantifies that the wave front curvature is reduced by a factor of 3.7 in the presence of the crescent-moon-like TiO_2 carpet.

Ref. 126 clearly demonstrates how transformation optics can be applied to mold the flow of SPPs. If following the traditional approach, we need to place dielectric nanostructures on metals or structure metal surfaces to realize the transformation plasmonic devices, similar to the employment of other various plasmonic elements. However, the abrupt discontinuities in the material properties or geometries of these elements lead to considerable scattering of SPPs, which significantly limits the device performance. Instead of spatially modifying the refractive index of the dielectric material, the thickness of a homogeneous dielectric cladding layer can be varied to change the effective mode index of SPPs. It provides an alternative method to realize transformation plasmonic devices. Using grey-scale electron-beam lithography (EBL) to adiabatically tailor the thickness of a thin dielectric ($\varepsilon = 2.19$) poly(methyl methacrylate) (PMMA) film adjacent to a metal surface, Zhang's group has demonstrated a plasmonic Luneburg lens to focus SPPs and a plasmonic Eaton lens to bend SPPs.[127] Fig. 9(a) shows the SEM image of one fabricated plasmonic Luneburg lens. A PMMA cone structure on top of a gold surface can achieve the required index profile of the traditional Luneburg lens given by $n(r) = \sqrt{2 - (r/R)^2}$, where R is the radius of the lens and r is the distance to the center. The 3D full wave simulation of the plasmonic Luneburg lens is presented in Fig. 9(b). In analogy to the traditional Luneburg lens, plane-wave-like SPPs launched from the left-hand side can be focused to a point on the opposite side of the perimeter of the PMMA cone base. Furthermore, because the optical properties are changed gradually rather than abruptly in the geometry, losses due to scattering can be significantly reduced in comparison with previously reported plasmonic elements. Fluorescence imaging and leakage radiation microscopy are applied to characterize the performance of the plasmonic Luneburg lenses, confirming the focusing effect over a relative broad wavelength range (Fig. 9(c)). The approach introduced in ref. 127 has the potential to achieve low-loss functional plasmonic elements with a standard fabrication technology based on the grey-scale electron-beam lithography, and could enable more complex 2D plasmonic elements using transformation optics.

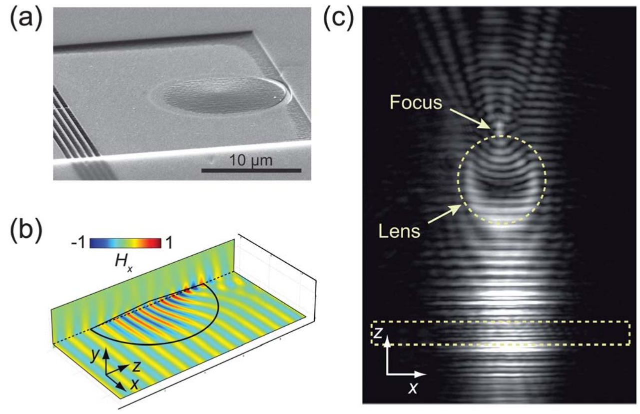

Fig. 9 (a) An SEM image of a plasmonic Luneburg lens made of PMMA on top of a gold film. The diameter and height of the lens are about 13 μm and 200 nm, respectively. (b) The plot of the magnetic field for SPPs propagating along the z-axis, which is focused to a point on the perimeter of the plasmonic Luneburg lens. (c) The intensity image obtained by leakage radiation microscopy for SPPs passing a Luneburg lens for wavelengths of 770 nm. SPPs are launched from a gold grating (dashed box) towards the Luneburg lens (dashed circle). Reprinted from ref. 127 with permission.

On the basis of conformal transformation, Pendry's group has provided an elegant framework for designing plasmonic nanostructures with remarkable properties over a broadband spectrum.[128] The general strategy is to start with an infinite plasmonic geometry that naturally shows a broadband spectrum, and then apply a conformal coordinate transformation that converts the infinite structure into a finite one while preserving the continuous spectrum.

One simple example is presented in Fig. 10(a). A point dipole is located between two semi-infinite slabs of metal. Due to the near-field components of the dipole radiation, SPPs can be excited and propagate along the metal surface. Now we apply a conformal mapping

$$z' = g^2/z^* \tag{10}$$

where g is a constant, $z = x + i \times y$ is the complex number notation and z^* represents the conjugate of z. Such a coordinate transformation translates the infinity points in z to the origin in

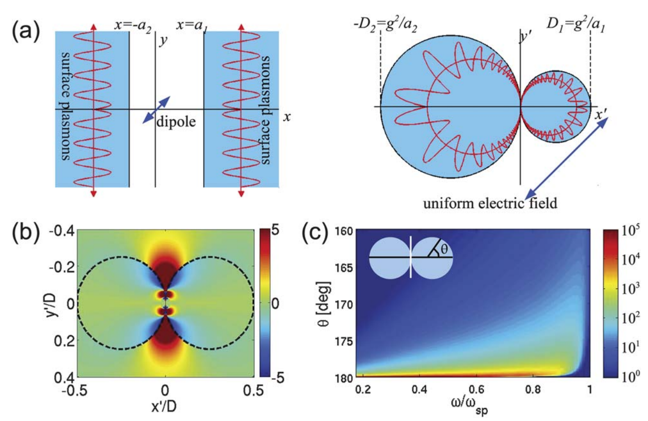

Fig. 10 (a) An example of conformal mapping that transforms two semi-infinite metallic slabs to two kissing-cylinders. Meanwhile, a dipole source at the origin is transformed to a uniform electric field. The surface plasmon modes initially propagating along the metal surfaces are folded and squeezed toward the touching point of kissing cylinders, while maintaining the continuous and broadband spectrum. (b) The amplitude of the x'-component of the electric field normalized by the uniform excitation field for silver at $\omega = 0.9\omega_{sp}$. The field amplitude around the touching point of the kissing cylinders is extremely high, although the color scale is restricted to [−5 5]. (c) The absolute value of the field enhancement, $|E'|/E_0$, along the cylinder surface as a function of the angle θ and frequency for a plane wave incident normal to the axis of the cylinders. Considerable field enhancement and confinement can be achieved over a broad spectrum range. Reprinted from ref. 128 with permission.

z', and translates planes into cylinders. The resulting structure is two kissing cylinders with the diameters of $D_1 = g^2/a_1$ and $D_2 = g^2/a_2$, respectively. The dipole source very close to the origin in z is translated to near infinity in z', giving rise to a uniform electric field excitation with respect to the kissing cylinders. Assuming the original dipole has strength Δ, the electric field at the origin in the transformed frame is then given by

$$E_0(z' = 0) = \frac{1}{2\pi\varepsilon_0}\frac{\Delta}{g^2} \quad (11)$$

If the dimension of the kissing cylinders is sufficiently small compared with the wavelength of interest, the quasi-static approximation can be applied. In this case, the magnetic field is decoupled with the electric field, and the dielectric properties of the transformed geometry (cylinders and the surrounding medium) are the same as the original ones from which they are derived. This is a very intriguing property of deep subwavelength structures after conformal mapping, which closely links the physics at work in each of the very different geometries. Although the material property is unchanged, the plasmon mode behaves rather differently in the two geometries. Before the transformation, the dipole excites surface plasmon modes on the metallic slabs that transport the energy out to the infinity without reflection. After the transformation, the same modes are excited by a uniform electric field E_0 (eqn (11)), and propagate to the origin in an adiabatic manner. Approaching the structure singularity (touching point), the wavelength of surface plasmons is shortened and the field is significantly enhanced due to the geometry folding (Fig. 10(b)). For an ideal lossless metal, surface plasmons accumulate energy toward the touching point but never reach it, since the plasmon modes excited in the original slab never reach infinity in a finite time. In practice, the finite loss introduces energy dissipation, but the maximum field enhancement can be still over 10^4 times in the vicinity of the touching point. Such a giant field enhancement will be extremely useful in a Raman scattering experiment at the single molecule level. The enhancement decreases due to a larger damping approaching the surface plasmon frequency, because surface plasmons are absorbed before having reached the touching point. Nevertheless, the simulation shows the enhancement over a broadband spectrum (Fig. 10(c)).

Applying different conformation transformations, researchers have explored a number of novel plasmonic geometries, such as nano crescents,[128] sharp wedges[129] and touching spheres,[130] which exhibit broadband response and prominent field enhancement at the geometry singularity. Moreover, detailed studies have been conducted to elucidate other relevant properties associated with plasmonic nanostructures. For instance, by taking into account radiation damping, Aubry *et al.* have extended the conformal transformation approach to predict the optical response of the plasmonic nanostructures beyond the quasi-static limit.[131] It is found that the radiative losses can be mapped directly onto the power dissipated by a fictive absorbing particle in the original frame. Radiative losses limit the maximum light enhancement capability but improve its broadband feature. The field enhancement is shown to decrease with the structure dimension, while still remaining in the order of 10^3 over the near-infrared and visible spectra. In addition, an insightful transformation optics approach has been developed to investigate the influence of the nonlocal effect on the optical properties of plasmonic nanostructures.[132] The light-harvesting performance of a dimer of touching nanowires is studied by using the hydrodynamical Drude model, which reveals nonlocal resonances not predicted by previous local calculations. Based on the hydrodynamical Drude model, the interplay between radiative and nonlocal effects is explored in touching nanowires, allowing us to optimize the geometry for maximizing the absorption and field enhancement.

Besides metals, graphene, a one-atom-thick planar sheet of sp^2-bonded carbon atoms, is able to support SPPs in the terahertz and infrared region.[133–135] Such a SPP wave is tightly confined to a single graphene layer, with a guided wavelength much smaller than free space wavelength, whereas its propagation distance could be large. The most important advantage of graphene for plasmonic applications over noble metals, such as silver and gold, is the capability to tune the conductivity and hence the permittivity of graphene by chemical doping or bias voltage dynamically and locally (Fig. 11(a) and (b)). As a result, we can realize the desired permittivity profiles across the graphene layer to achieve many flatland plasmonic devices.[136] As an example of transformation plasmonic devices, a "flat" version of a Luneburg lens is presented in Fig. 11(c). With a special configuration of bias arrangement in the manner of several concentric rings, we can create, approximately, a gradient conductivity pattern that provides the required effective index for the graphene-based Luneburg lens. Specifically, the conductivity follows the expression $\sigma_{i,n} = \sigma_{i,out}\{2 - [(r_n + r_{n-1})/D]^2\}^{-1/2}$, where $\sigma_{i,n}$ and r_n represent the imaginary part of the conductivity and the radius of the n^{th} section, and $\sigma_{i,out}$ is the imaginary part of the conductivity of the background

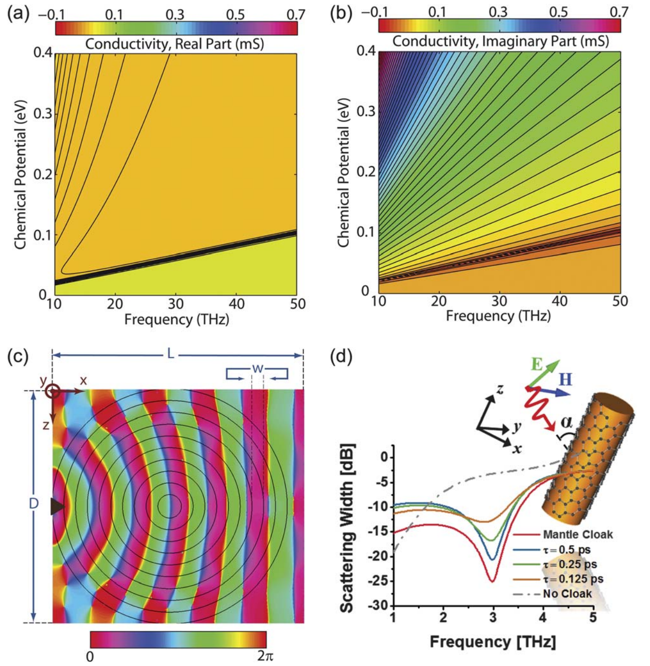

Fig. 11 (a) The real part and (b) the imaginary part of the conductivity of a free-standing graphene as a function of the chemical potential and frequency. (c) The simulated phase of SPPs at $f = 30$ THz along the graphene-based Luneburg lens ($D = 1.5$ μm, $w = 75$ nm, $L = 1.6$ μm). The black triangle indicates the position of the point source. (a)–(c) are reprinted from ref. 136 with permission. (d) The scattering width of an infinite dielectric cylinder with diameter $D = \lambda_0/5$ and relative permittivity $\varepsilon_d = 3.9$ under different conditions. The red line represents an ideal lossless mantle cloak with surface reactance $X_s = 313\ \Omega$ (red line). Graphene surface cloaks with a chemical potential of 0.51 eV and different values of momentum relaxation time τ are shown in blue, green, and yellow lines. The momentum relaxation time is inverse to the electron–phonon scattering rate. The dashed line corresponds to the bare cylinder without a cloak. Reprinted from ref. 141 with permission.

graphene. The simulation reveals that the SPPs generated from a point source is evolved into an approximately "collimated beam" of SPPs on the one-atom-thick graphene, as a conventional 3D Luneburg lens collimates wavefronts generated from a point source into a 3D beam. The diameter of the "flat" Luneburg lens is about 1.5 μm, which is only one-tenth of the wavelength. We can also design other subwavelength graphene-based optical devices, including lenses,[137,138] nanoribbon plasmonic waveguides,[139,140] and surface cloaks,[141] implying that graphene provides a versatile platform for electro-optics and transformation optics at the atom scale. In ref. 141, it is numerically demonstrated that an atomically thin graphene monolayer may drastically suppress the scattering of a cylindrical object over a moderately broad bandwidth in the terahertz regime (Fig. 11(d)). In addition, the working frequency of the surface cloak may be largely tuned by varying the chemical potential, realizing a tunable and switchable cloaking device.

7. Future directions

So far, transformation optics has been focusing on the spatial control of the light path. From a mathematical point of view, the spatial and temporal evolutions of light share certain similarities. Therefore, it will be feasible and intriguing to extend the concept of transformation optics to the temporal domain. For instance, instead of rendering an object invisible by a spatial invisibility cloak, we may create a temporal cloak to hide the occurrence of an event within a well-controlled time gap as recently proposed by McCall *et al.*[142] Such a time gap can be opened by manipulating the dispersion of materials in time, so that the front and rear parts of a probe light beam are accelerated and slowed down, respectively. An event, such as the incidence of a pump beam, which occurs within the resulting temporal gap, would not modify the probe beam in any case. Subsequently, the time gap can be closed by the reverse manipulation of the dispersion and thus the speed light. When the restored probe light reaches an observer, it appears as a continuous, uniform light as if the event has never occurred. The experimental demonstration of temporal cloaking utilizes time lenses and dispersive media.[143] A time lens can change the colour of the probe light beam at different moments in time, *via* electro-optic modulation or parametric nonlinear optical processes such as four-wave mixing with a chirped pump wave. Then the "red" and "blue" parts of the chirped probe beam are transferred to the edges of the time window through an optical fibre due to dispersion. Consequently, a time gap is generated and any event within this gap that might produce a temporal or spectral change to the probe beam will have no effect. Finally, a dispersive-compensating optical fibre together with another time lens is used to close the time gap. The result is that neither the occurrence of the event nor the presence of the time-lenses is perceivable to an observer. The experimental demonstration in ref. 143 is essentially a 1D temporal cloak. Future directions may include temporal cloaking working for arbitrary incident angles, or even full spatial–temporal transformation optical devices.

The geometric transformation approach can be extended to other systems beyond electromagnetic waves, as long as the governing equations for these systems are invariant under coordinate transformations. Along this direction, significant effort has been devoted to transforming acoustic waves[144–148] elastic waves in thin plates,[149,150] linear surface liquid waves[151,152] and fluid flows.[153] Even in the quantum mechanics regime, it is possible to transform matter waves,[154–156] the wave description of particles like electrons and neutrons. For instance, Zhang *et al.* theoretically designed an invisibility cloak for matter waves based on time-invariant coordinate transformations of Schrödinger's equations.[154] The cloak is a 3D optical lattice of laser beams, forming optical standing waves with gradually varying amplitude along the radial direction. The varying amplitude of the optical lattice changes the effective mass and band energy of the incident particles, which cause the stream of particles or incident matter waves to bend and come out on the exit side as if no objects were present in the center. The experimental demonstration of 3D quantum wave cloaks will be extremely challenging. However, a 2D version of such cloaks may be possible *via* electric bias to control the effective mass of electrons on a graphene sheet. By examining a graphene p–n junction, Cheianov *et al.* numerically show that a point source of electron currents in the n-type region radiates electrons to the interface, where they are negatively refracted into the p-type region and brought to a focus. This is just in analogy to light focused by a slab of negative index materials.[157]

The recent progress on nonlinear and tunable metamaterials promises the further development of transformation optical structures. Up to now, almost all the implementations of transformation optics have relied on passive and linear metamaterials. It has been proposed that using active sources rather than passive materials could achieve cloaking, similar to the active control of sound for noise suppression.[158,159] Although active-source cloaking has certain advantages in terms of fabrication and bandwidth, but the technique is very challenging at optical frequencies. In contrast, nonlinear and tunable metamaterials may be the ultimate approach for realizing active transformation optical devices, such as invisibility cloaks which can be turned on and off by external fields. Since the early stage of metamaterial research, nonlinear metamaterials have attracted continuous attention due to their novel properties and phenomena.[64,160–164] The experimental demonstrations associated with nonlinear metamaterials, including tunable split-ring resonators,[165] second harmonic generation,[166,167] negative refraction arising from phase conjugation[168] and four-wave mixing[169] as well as magnetoelastic metamaterials,[170] manifest a very bright future towards actively tunable transformation optical devices. The proof-of-principle experiments at microwave wavelengths should be feasible. In the optical region, the major issue of material losses could be overcome by incorporating gain media into metamaterials.[171–176] Very recently, Yang *et al.* have demonstrated that a laminar liquid flow in an optofluidic channel exhibits spatially variable dielectric properties depending on the flow rate, allowing for chirped focusing of light and distinctive discrete diffraction.[177] In addition, it has been shown that electric or magnetic fields can control the spatial distribution and orientation of metallic nanostructures suspended in fluids.[178,179] These results indicate that optofluidic systems may provide a new platform for controllable or even reconfigurable transformation optical devices.

8. Conclusions

Rooted in electromagnetism, an ancient subject existing over centuries, transformation optics has opened an unprecedented avenue towards the ultimate control over light flow at will. Driven by the rapid development of metamaterials and start-of-the-art nanofabrication techniques, many remarkable transformation optical devices have been realized in the optical domain soon after proof-of-concept demonstrations at low frequencies. Nowadays we can really visualize the invisibility effect, which had been thought magical for a long time, even with the naked eye. Many other fascinating aspects of transformation optics and its extensions are rising from the horizon, such as the temporal control of light waves, tunable and reconfigurable transformation optical devices and the manipulation of other waves including quantum waves. The ideas in transformation optics are far from exhausted. As nanophotonics and nanotechnology are moving forward, we can make more seemingly impossible things into reality with the versatile methodology of transformation optics.

Acknowledgements

The authors are grateful for the financial support from the United States Army Research Office MURI program under grant number W911NF-09-1-0539 and the NSF Nano-scale Science and Engineering Center (NSEC) under grant number CMMI-0751621.

References

1 M. Born and E. Wolf, *Principles of Optics*, Cambridge University Press, Cambridge, UK, 1999.
2 J. B. Pendry, D. Schurig and D. R. Smith, Controlling electromagnetic fields, *Science*, 2006, **312**, 1780–1782.
3 U. Leonhardt and T. G. Philbin, Transformation optics and the geometry of light, *Prog. Opt.*, 2009, **53**, 69–152.
4 H. Y. Chen, C. T. Chan and P. Sheng, Transformation optics and metamaterials, *Nat. Mater.*, 2010, **9**, 387–396.
5 G. W. Milton, M. Briane and J. R. Willis, On cloaking for elasticity and physical equations with a transformation invariant form, *New J. Phys.*, 2006, **8**, 248.
6 D. Schurig, J. B. Pendry and D. R. Smith, Calculation of material properties and ray tracing in transformation media, *Opt. Express*, 2006, **14**, 9794–9804.
7 S. A. Cummer, B.-I. Popa, D. Schurig, D. R. Smith and J. B. Pendry, Full-wave simulations of electromagnetic cloaking structures, *Phys. Rev. E: Stat., Nonlinear, Soft Matter Phys.*, 2006, **74**, 036621.
8 U. Leonhardt, Optical conformal mapping, *Science*, 2006, **312**, 1777–1780.
9 U. Leonhardt, Notes on conformal invisibility devices, *New J. Phys.*, 2006, **8**, 118.
10 U. Leonhardt and T. Tyc, Broadband invisibility by non-euclidean cloaking, *Science*, 2009, **323**, 110–112.
11 N. I. Landy and W. J. Padilla, Guiding light with conformal transformations, *Opt. Express*, 2009, **17**, 14872–14879.
12 J. P. Turpin, A. T. Massoud, Z. H. Jiang, P. L. Werner and D. H. Werner, Conformal mappings to achieve simple material parameters for transformation optics devices, *Opt. Express*, 2010, **18**, 244–252.
13 B. Vasic, G. Isic, R. Gajic and K. Hingerl, Controlling electromagnetic fields with graded photonic crystals in metamaterial regime, *Opt. Express*, 2010, **18**, 20321–20333.
14 M. Schmiele, V. S. Varma, C. Rockstuhl and F. Lederer, Designing optical elements from isotropic materials by using transformation optics, *Phys. Rev. A: At., Mol., Opt. Phys.*, 2010, **81**, 033837.
15 K. Yao and X. Y. Jiang, Designing feasible optical devices *via* conformal mapping, *J. Opt. Soc. Am. B*, 2011, **28**, 1037–1042.
16 T. Tyc, H. Y. Chen, C. T. Chan and U. Leonhardt, Non-euclidean cloaking for light waves, *IEEE J. Sel. Top. Quantum Electron.*, 2010, **16**, 418–426.
17 A. Alù and N. Engheta, Achieving transparency with plasmonic and metamaterial coating, *Phys. Rev. E: Stat., Nonlinear, Soft Matter Phys.*, 2005, **72**, 016623.
18 B. Edward, A. Alù, M. Silveirinha and N. Engheta, Experimental verification of plasmonic cloaking at microwave frequencies with metamaterials, *Phys. Rev. Lett.*, 2009, **103**, 153901.
19 A. Alù and N. Engheta, *Phys. Rev. Lett.*, 2008, **100**, 113901.
20 H. S. Chen, B. I. Wu, B. L. Zhang and J. A. Kong, Electromagnetic wave interactions with a metamaterial cloak, *Phys. Rev. Lett.*, 2007, **99**, 063903.
21 Z. C. Ruan, M. Yan, C. W. Neff and M. Qiu, Ideal cylindrical cloak: perfect but sensitive to tiny perturbations, *Phys. Rev. Lett.*, 2007, **99**, 113903.
22 M. Yan, Z. C. Ruan and M. Qiu, Cylindrical invisibility cloak with simplified material parameters is inherently visible, *Phys. Rev. Lett.*, 2007, **99**, 233901.
23 B. L. Zhang, H. S. Chen, B. I. Wu and J. A. Kong, Extraordinary surface voltage effect in the invisibility cloak with an active device inside, *Phys. Rev. Lett.*, 2008, **100**, 063904.
24 H. Hashemi, B. L. Zhang, J. D. Joannopoulos and S. G. Johnson, Delay-bandwidth and delay-loss limitations for cloaking of large objects, *Phys. Rev. Lett.*, 2010, **104**, 253903.

25 H. Y. Chen, X. D. Luo, H. R. Ma and C. T. Chan, The anti-cloak, *Opt. Express*, 2008, **16**, 14603–14608.
26 B. L. Zhang and B. I. Wu, Electromagnetic detection of a perfect invisibility cloak, *Phys. Rev. Lett.*, 2009, **103**, 243901.
27 Y. Lai, J. Ng, H. Y. Chen, D. Z. Han, J. J. Xiao, Z. Q. Zhang and C. T. Chan, Illusion optics: the optical transformation of an object into another object, *Phys. Rev. Lett.*, 2009, **102**, 253902.
28 W. X. Jiang, H. F. Ma, Q. Cheng and T. J. Cui, Illusion media: generating virtual objects using realizable metamaterials, *Appl. Phys. Lett.*, 2010, **96**, 121910.
29 X. D. Luo, T. Yang, Y. W. Gu, H. Y. Chen and H. R. Ma, Conceal an entrance by means of superscatter, *Appl. Phys. Lett.*, 2009, **94**, 223513.
30 C. Li, X. Meng, X. Liu, F. Li, G. Y. Fang, H. Y. Chen and C. T. Chan, Experimental realization of a circuit-based broadband illusion-optics analogue, *Phys. Rev. Lett.*, 2010, **105**, 233906.
31 U. Leonhardt and P. Piwnicki, Optics of nonuniformly moving media, *Phys. Rev. A: At., Mol., Opt. Phys.*, 1999, **60**, 4301–4312.
32 D. A. Genov, S. Zhang and X. Zhang, Mimicking celestial mechanics in metamaterials, *Nat. Phys.*, 2009, **5**, 687–692.
33 E. E. Narimanov and A. V. Kildishev, Optical black hole: broadband omnidirectional light absorber, *Appl. Phys. Lett.*, 2009, **95**, 041106.
34 Q. Cheng, T. J. Cui, W. X. Jiang and B. G. Cai, An omnidirectional electromagnetic absorber made of metamaterials, *New J. Phys.*, 2010, **12**, 063006.
35 M. Rahm, S. A. Cummer, D. Schurig, J. B. Pendry and D. R. Smith, Optical design of reflectionless complex media by finite embedded coordinate transformations, *Phys. Rev. Lett.*, 2008, **100**, 063903.
36 H. Y. Chen and C. T. Chan, Transformation media that rotate electromagnetic fields, *Appl. Phys. Lett.*, 2007, **90**, 241105.
37 H. Y. Chen, B. Hou, S. Y. Chen, X. Y. Ao, W. J. Wen and C. T. Chan, Design and experimental realization of a broadband transformation media field rotator at microwave frequencies, *Phys. Rev. Lett.*, 2009, **102**, 183903.
38 D. R. Roberts, M. Rahm, J. B. Pendry and D. R. Smith, Transformation-optical design of sharp waveguide bends and corners, *Appl. Phys. Lett.*, 2008, **93**, 251111.
39 D. H. Kwon and D. H. Werner, Transformation optical designs for wave collimators, flat lenses and right-angle bends, *New J. Phys.*, 2008, **10**, 115023.
40 J. T. Huangfu, S. Xi, F. M. Kong, J. J. Zhang, H. S. Chen, D. X. Wang, B. I. Wu, L. X. Ran and J. A. Kong, Application of coordinate transformation in bent waveguides, *J. Appl. Phys.*, 2008, **104**, 014502.
41 Z. L. Mei and T. J. Cui, Arbitrary bending of electromagnetic waves using isotropic materials, *J. Appl. Phys.*, 2009, **105**, 104913.
42 D. Schurig, J. B. Pendry and D. R. Smith, Transformation-designed optical elements, *Opt. Express*, 2007, **15**, 14772–14782.
43 A. V. Kildishev and V. M. Shalaev, Engineering space for light *via* transformation optics, *Opt. Lett.*, 2008, **33**, 43–45.
44 M. Yan, W. Yan and M. Qiu, Cylindrical superlens by a coordinate transformation, *Phys. Rev. B: Condens. Matter Mater. Phys.*, 2008, **78**, 125113.
45 M. Tsang and D. Psaltis, Magnifying perfect lens and superlens designed by coordinate transformation, *Phys. Rev. B: Condens. Matter Mater. Phys.*, 2008, **77**, 035122.
46 Y. K. Ma, C. K. Ong, T. Tyc and U. Leonhardt, An omnidirectional retroreflector based on the transmutation of dielectric singularities, *Nat. Mater.*, 2009, **8**, 639–642.
47 D. A. Roberts, N. Kundtz and D. R. Smith, Optical lens compression *via* transformation optics, *Opt. Express*, 2009, **17**, 16535–16542.
48 N. Kundtz and D. R. Smith, Extreme-angle broadband metamaterial lens, *Nat. Mater.*, 2010, **9**, 129–132.
49 H. F. Ma and T. J. Cui, Three-dimensional broadband and broad-angle transformation-optics lens, *Nat. Commun.*, 2010, **1**, 124.
50 Z. H. Jiang, M. D. Gregory and D. H. Werner, Experimental demonstration of a broadband transformation optics lens for highly directive multibeam emission, *Phys. Rev. B: Condens. Matter Mater. Phys.*, 2011, **84**, 165111.
51 J. B. Pendry and S. A. Ramakrishna, Focusing light using negative refraction, *J. Phys.: Condens. Matter*, 2003, **15**, 6345–6364.
52 T. Yang, H. Y. Chen, X. D. Luo and H. R. Ma, Superscatter: enhancement of scattering with complementary media, *Opt. Express*, 2008, **16**, 18545–18550.
53 Y. Lai, H. Y. Chen, Z. Q. Zhang and C. T. Chan, Complementary media invisibility cloak that cloaks objects at a distance outside the cloaking shell, *Phys. Rev. Lett.*, 2009, **102**, 093901.
54 D. R. Smith, J. B. Pendry and M. C. K. Wiltshire, Metamaterials and negative refractive index, *Science*, 2004, **305**, 788–792.
55 V. M. Shalaev, Optical negative-index metamaterials, *Nat. Photonics*, 2007, **1**, 41–48.
56 M. Wegener and S. Linden, Shaping optical space with metamaterials, *Phys. Today*, 2010, **63**, 32–36.
57 Y. M. Liu and X. Zhang, Metamaterials: a new frontier of science and technology, *Chem. Soc. Rev.*, 2011, **40**, 2494–2507.
58 C. M. Soukoulis and M. Wegener, Past achievements and future challenges in the development of three-dimensional photonic metamaterials, *Nat. Photonics*, 2011, **5**, 523–530.
59 N. Engheta and R. W. Ziolkowski, *Electromagnetic Metamaterials: Physics and Engineering Explorations*, Wiley-IEEE Press, 1st edn, 2006.
60 W. S. Cai and V. M. Shalaev, *Optical Metamaterials: Fundamentals and Applications*, Springer, New York, 1st edn, 2009.
61 T. J. Cui, D. R. Smith and R. P. Liu, *Metamaterials: Theory, Design, and Applications*, Springer, 1st edn, 2009.
62 A. Sihvola, *Electromagnetic Mixing Formulas and Applications*, Institution of Electrical Engineers, 1999.
63 J. B. Pendry, A. J. Holden, W. J. Stewart and I. Youngs, *Phys. Rev. Lett.*, 1996, **76**, 4773–4776.
64 J. B. Pendry, A. J. Holden, D. J. Robbins and W. J. Stewart, *IEEE Trans. Microwave Theory Tech.*, 1999, **47**, 2075–2084.
65 D. R. Smith, W. J. Padilla, D. C. Vier, S. C. Nemat-Nasser and S. Schultz, *Phys. Rev. Lett.*, 2000, **84**, 4184–4187.
66 R. A. Shelby, D. R. Smith and S. Schultz, *Science*, 2001, **292**, 77–79.
67 C. G. Parazzoli, R. B. Greegor, K. Li, B. E. C. Koltenbah and M. Tanielian, Experimental verification and simulation of negative index of refraction using Snell's law, *Phys. Rev. Lett.*, 2003, **90**, 107401.
68 S. Zhang, W. J. Fan, N. C. Panoiu, K. J. Malloy, R. M. Osgood and S. R. J. Brueck, Experimental demonstration of near-infrared negative-index metamaterials, *Phys. Rev. Lett.*, 2005, **95**, 137404.
69 J. Valentin, S. Zhang, T. Zentgraf, E. Ulin-Avila, D. A. Genov, G. Bartal and X. Zhang, Three-dimensional optical metamaterial with a negative refractive index, *Nature*, 2008, **455**, 376–379.
70 J. B. Pendry, Negative refraction makes a perfect lens, *Phys. Rev. Lett.*, 2000, **85**, 3966–3969.
71 A. N. Lagarkov and V. N. Kissel, Near-perfect imaging in a focusing system based on a left-handed-material plate, *Phys. Rev. Lett.*, 2004, **92**, 077401.
72 N. Fang, H. Lee, C. Sun and X. Zhang, Sub-diffraction-limited optical imaging with a silver superlens, *Science*, 2005, **308**, 534–537.
73 T. Taubner, D. Korobkin, Y. Urzhumov, G. Shvets and R. Hillenbrand, Near-field microscopy through a SiC superlens, *Science*, 2006, **313**, 1595.
74 X. Zhang and Z. W. Liu, Superlenses to overcome the diffraction limit, *Nat. Mater.*, 2008, **7**, 435–441.
75 D. R. Smith, D. Schurig, J. J. Mock, P. Kolinko and P. Rye, Partial focusing of radiation by a slab of indefinite media, *Appl. Phys. Lett.*, 2004, **84**, 2244–2246.
76 A. J. Hoffman, *et al.*, Negative refraction in semiconductor metamaterials, *Nat. Mater.*, 2007, **6**, 946–950.
77 J. Yao, Z. W. Liu, Y. M. Liu, Y. Wang, C. Sun, G. Bartal, A. M. Stacy and X. Zhang, Optical negative refraction in bulk metamaterials of nanowires, *Science*, 2007, **321**, 930.
78 S. Zhang, Y. Park, J. S. Li, X. C. Lu, W. L. Zhang and X. Zhang, Negative refractive index in chiral metamaterials, *Phys. Rev. Lett.*, 2009, **102**, 023901.
79 E. Plum, J. Zhou, J. Dong, V. A. Fedotov, T. Koschny, C. M. Soukoulis and N. I. Zheludev, Metamaterial with negative index due to chirality, *Phys. Rev. B: Condens. Matter Mater. Phys.*, 2009, **79**, 035407.
80 J. K. Gansel, *et al.*, Gold helix photonic metamaterial as broadband circular polarizer, *Science*, 2009, **325**, 1513–1515.
81 D. Schurig, J. J. Mock, B. J. Justice, S. A. Cummer, J. B. Pendry, A. F. Starr and D. R. Smith, Metamaterial electromagnetic cloak at microwave frequencies, *Science*, 2006, **314**, 977–980.

82 W. S. Cai, U. K. Chettiar, A. V. Kildishev and V. M. Shalaev, Optical cloaking with metamaterials, *Nat. Photonics*, 2007, **1**, 224–227.

83 J. S. Li and J. B. Pendry, Hiding under the carpet: a new strategy for cloaking, *Phys. Rev. Lett.*, 2008, **101**, 203901.

84 H. Y. Chen and C. T. Chan, Electromagnetic wave manipulation by layered systems using the transformation media concept, *Phys. Rev. B: Condens. Matter Mater. Phys.*, 2008, **78**, 054204.

85 S. Xi, H. S. Chen, B. I. Wu and J. A. Kong, One-directional perfect cloak created with homogeneous material, *IEEE Microwave and Wireless Components Letters*, 2009, **19**, 131–133.

86 R. Liu, C. Ji, J. J. Mock, J. Y. Chin, T. J. Cui and D. R. Smith, Broadband ground-plane cloak, *Science*, 2009, **323**, 366–369.

87 J. Valentine, J. Li, T. Zentgraf, G. Bartal and X. Zhang, An optical cloak made of dielectrics, *Nat. Mater.*, 2009, **7**, 568–571.

88 L. H. Gabrielli, J. Cardenas, C. B. Poitras and M. Lipson, Silicon nanostructure cloak operating at optical frequencies, *Nat. Photonics*, 2009, **43**, 461–463.

89 J. H. Lee, J. Blair, V. A. Tamma, Q. Wu, S. J. Rhee, C. J. Summers and W. Park, Direct visualization of optical frequency invisibility cloak based on silicon nanorod array, *Opt. Express*, 2009, **17**, 12922–12928.

90 T. Ergin, N. Stenger, P. Brenner, J. B. Pendry and M. Wegener, Three-dimensional invisibility cloak at optical wavelengths, *Science*, 2010, **328**, 337–339.

91 T. Ergin, J. C. Halimeh, N. Stenger and M. Wegener, Optical microscopy of 3D carpet cloaks: ray-tracing calculations, *Opt. Express*, 2010, **18**, 20535–20545.

92 Y. A. Urzhumov and D. R. Smith, Transformation optics with photonic band gap media, *Phys. Rev. Lett.*, 2010, **105**, 163901.

93 Z. X. Liang and S. J. Li, Scaling two-dimensional photonic crystals for transformation optics, *Opt. Express*, 2011, **19**, 16821–16829.

94 E. Cassan and K.-V. Do, Analytic design of graded photonic crystals in the metamaterial regime, *J. Opt. Soc. Am. B*, 2011, **28**, 1905.

95 J. Fischer, T. Ergin and M. Wegener, Three-dimensional polarization-independent visible-frequency carpet invisibility cloak, *Opt. Lett.*, 2011, **36**, 2059–2061.

96 J. Fischer and M. Wegener, Three-dimensional direct laser writing inspired by stimulated-emission-depletion microscopy, *Opt. Mater. Express*, 2011, **1**, 614–624.

97 T. Ergin, J. Fischer and M. Wegener, Optical phase cloaking of 700 nm light waves in the far field by a three-dimensional carpet cloak, *Phys. Rev. Lett.*, 2011, **107**, 173901.

98 M. Charghi, C. Gladden, T. Zentgraf, Y. M. Liu, X. B. Yin, J. Valentine and X. Zhang, A carpet cloak for visible light, *Nano Lett.*, 2011, **11**, 2825–2828.

99 T. Zentgraf, J. Valentine, N. Tapia, J. S. Li and X. Zhang, An optical "Janus" device for integrated photonics, *Adv. Mater.*, 2010, **22**, 2561–2564.

100 A. Di Falco, S. C. Kehr and U. Leonhardt, Luneburg lens in silicon photonics, *Opt. Express*, 2011, **19**, 5156–5162.

101 J. Hunt, T. Tyler, S. Dhar, Y. J. Tsai, P. Bowen, S. Larouche, N. M. Jokerst and D. R. Smith, Planar, flattened Luneburg lens at infrared wavelengths, *Opt. Express*, 2012, **20**, 1706–1713.

102 L. H. Gabrielli and M. Lipson, Integrated Luneburg lens *via* ultra-strong index gradient on silicon, *Opt. Express*, 2011, **19**, 20122–20127.

103 H. F. Ma and T. J. Cui, Three-dimensional broadband ground-plane cloak made of metamaterials, *Nat. Commun.*, 2010, **1**, 21.

104 F. Zhou, Y. J. Bao, W. Cao, C. T. Stuart, J. Q. Gu, W. L. Zhang and C. Sun, Hiding realistic object using a broadband terahertz invisibility cloak, *Sci. Rep.*, 2011, **1**, 78.

105 D. H. Liang, J. Q. Gu, J. G. Han, Y. M. Yang, S. Zhang and W. L. Zhang, Robust large dimension terahertz cloaking, *Adv. Mater.*, 2012, **24**, 916–921.

106 X. Z. Chen, Y. Luo, J. J. Zhang, K. Jiang, J. B. Pendry and S. Zhang, Macroscopic invisibility cloaking of visible light, *Nat. Commun.*, 2011, **2**, 176.

107 B. L. Zhang, Y. Luo, X. G. Liu and G. Barbastathis, Macroscopic invisibility cloak for visible light, *Phys. Rev. Lett.*, 2011, **106**, 033901.

108 B. L. Zhang, T. Chan and B. I. Wu, Lateral shift makes a ground-plane cloak detectable, *Phys. Rev. Lett.*, 2010, **104**, 233903.

109 H. S. Chen and B. Zheng, Broadband polygonal invisibility cloak for visible light, *Sci. Rep.*, 2012, **2**, 255.

110 H. Raether, *Surface Plasmons: On Smooth and Rough Surfaces and on Gratings*, Springer, Berlin, 1988.

111 W. L. Barnes, A. Dereux and T. W. Ebbesen, Surface plasmon subwavelength optics, *Nature*, 2003, **424**, 824–830.

112 N. Engheta, Circuits with light at nanoscales: optical nanocircuits inspired by metamaterials, *Science*, 2007, **317**, 1698–1702.

113 D. K. Gramotnev and S. I. Bozhevolnyi, Plasmonics beyond the diffraction limit, *Nat. Photonics*, 2010, **4**, 83–91.

114 J. A. Schuller, E. S. Barnard, W. S. Cai, Y. C. Jun, J. S. White and M. L. Brongersma, Plasmonics for extreme light concentration and manipulation, *Nat. Mater.*, 2010, **9**, 193–204.

115 S. Kawata, Y. Inouye and P. Verma, Plasmonics for near-field nano-imaging and superlensing, *Nat. Photonics*, 2009, **3**, 388–394.

116 W. Srituravanich, N. Fang, C. Sun, Q. Luo and X. Zhang, Plasmonic nanolithography, *Nano Lett.*, 2004, **4**, 1085–1088.

117 W. Srituravanich, L. Pan, Y. Wang, C. Sun, D. B. Bogy and X. Zhang, Flying plasmonic lens in the near field for high-speed nanolithography, *Nat. Nanotechnol.*, 2008, **3**, 733–737.

118 W. A. Challener, *et al.*, Heat-assisted magnetic recording by a near-field transducer with efficient optical energy transfer, *Nat. Photonics*, 2009, **3**, 220–224.

119 B. C. Stipe, *et al.*, Magnetic recording at 1.5 Pb m^{-2} using an integrated plasmonic antenna, *Nat. Photonics*, 2010, **4**, 484–488.

120 J. N. Anker, W. P. Hall, O. Lyandres, N. C. Shah, J. Zhao and R. P. Van Duyne, Biosensing with plasmonic nanosensors, *Nat. Mater.*, 2008, **7**, 442–453.

121 N. J. Halas, Plasmonics: an emerging field fostered by Nano Letters, *Nano Lett.*, 2010, **10**, 3816–3822.

122 H. A. Atwater and P. Albert, *Nat. Mater.*, 2010, **9**, 205–213.

123 Y. M. Liu, T. Zentgraf, G. Bartal and X. Zhang, Transformational plasmon optics, *Nano Lett.*, 2010, **10**, 1991–1997.

124 P. A. Huidobro, M. L. Nesterov, L. Martín-Moreno and F. J. García-Vidal, Transformation optics for plasmonics, *Nano Lett.*, 2010, **10**, 1985–1990.

125 R. F. Oulton, D. F. P. Pile, Y. M. Liu and X. Zhang, Scattering of surface plasmon polaritons at abrupt surface interfaces: implications for nanoscale cavities, *Phys. Rev. B: Condens. Matter Mater. Phys.*, 2007, **76**, 035408.

126 J. Renger, M. Kadic, G. Dupont, S. S. Aćimović, S. Guenneau, R. Quidant and S. Enoch, Hidden progress: broadband plasmonic invisibility, *Opt. Express*, 2010, **18**, 15757–15768.

127 T. Zentgraf, Y. M. Liu, M. H. Mikkelsen, J. Valentine and X. Zhang, Plamonic Luneburg and Eaton lenses, *Nat. Nanotechnol.*, 2011, **6**, 151–155.

128 A. Aubry, D. Y. Lei, A. I. Fernández-Domínguez, Y. Sonnefraud, S. A. Maier and J. B. Pendry, Plasmonic light-harvesting devices over the whole visible spectrum, *Nano Lett.*, 2010, **10**, 2574–2579.

129 Y. Luo, J. B. Pendry and A. Aubry, Surface plasmons and singularities, *Nano Lett.*, 2010, **10**, 4186–4191.

130 A. I. Fernández-Domínguez, S. A. Maier and J. B. Pendry, Collection and concentration of light by touching spheres: a transformation optics approach, *Phys. Rev. Lett.*, 2010, **105**, 266807.

131 A. Aubry, D. Y. Lei, S. A. Maier and J. B. Pendry, Conformal transformation applied to plasmonics beyond the quasistatic limit, *Phys. Rev. B: Condens. Matter Mater. Phys.*, 2010, **82**, 205109.

132 A. I. Fernández-Domínguez, A. Wiener, F. J. García-Vidal, S. A. Maier and J. B. Pendry, Transformation-optics description of nonlocal effects in plasmonic nanostructures, *Phys. Rev. Lett.*, 2012, **108**, 106802.

133 M. Jablan, H. Buljan and M. Soljacic, Plasmonics in graphene at infrared frequencies, *Phys. Rev. B: Condens. Matter Mater. Phys.*, 2009, **80**, 245436.

134 L. Ju, *et al.*, Graphene plasmonics for tunable terahertz metamaterials, *Nat. Nanotechnol.*, 2011, **6**, 630–634.

135 H. G. Yan, X. S. Li, B. Chandra, G. Tulevski, Y. Q. Wu, M. Freitag, E. J. Zhu, P. Avouris and F. N. Xia, Tunable infrared plasmonic devices using graphene/insulator stacks, *Nat. Nanotechnol.*, 2012, **7**, 330–334.

136 A. Vakil and N. Engheta, Transformation optics using graphene, *Science*, 2011, **332**, 1291–1294.

137 H. J. Xu, W. B. Ju, Y. Jiang and Z. G. Dong, Beam-scanning planar lens based on graphene, *Appl. Phys. Lett.*, 2012, **100**, 051903.

138 A. Vakil and N. Engheta, Fourier optics on graphene, *Phys. Rev. B: Condens. Matter Mater. Phys.*, 2012, **85**, 075434.

139 A. Yu. Nikitin, F. Guinea, F. J. García-Vidal and L. Martín-Moreno, Edge and waveguide terahertz surface plasmon modes in graphene microribbons, *Phys. Rev. B: Condens. Matter Mater. Phys.*, 2011, **84**, 161407.
140 J. Christensen, A. Manjavacas, S. Thongrattanasiri, F. H. L. Koppens and F. J. García de Abajo, Graphene plasmon waveguiding and hybridization in individual and paired nanoribbons, *ACS Nano*, 2012, **6**, 431–440.
141 P. Y. Chen and A. Alu, Atomically thin surface cloak using graphene monolayers, *ACS Nano*, 2011, **5**, 5855–5863.
142 M. W. McCall, A. Favaro, P. Kinsler and A. Boardman, A spacetime cloak, or a history editor, *J. Opt.*, 2011, **13**, 024003.
143 M. Fridman, A. Farsi, Y. Okawachi and A. L. Gaeta, Demonstration of temporal cloaking, *Nature*, 2012, **481**, 62–65.
144 S. A. Cummer and D. Schurig, One path to acoustic cloaking, *New J. Phys.*, 2007, **9**, 45.
145 H. Chen and C. T. Chan, Acoustic cloaking in three dimensions using acoustic metamaterials, *Appl. Phys. Lett.*, 2007, **91**, 183518.
146 S. A. Cummer, B. I. Popa, D. Schurig, D. R. Smith, J. Pendry, M. Rahm and A. Starr, Scattering theory derivation of a 3D acoustic cloaking shell, *Phys. Rev. Lett.*, 2008, **100**, 024301.
147 S. Zhang, C. G. Xia and N. Fang, Broadband acoustic cloak for ultrasound waves, *Phys. Rev. Lett.*, 2011, **106**, 024301.
148 X. F. Zhu, B. Liang, W. W. Kan, X. Y. Zou and J. C. Cheng, Acousticcloaking by a superlens with sing-negative materials, *Phys. Rev. Lett.*, 2011, **106**, 014301.
149 M. Farhat, S. Guenneau and S. Enoch, Ultrabroadband elastic cloaking in thin plates, *Phys. Rev. Lett.*, 2009, **103**, 024301.
150 N. Stenger, M. Wilhelm and M. Wegener, Experiments on elastic cloaking in thin plates, *Phys. Rev. Lett.*, 2012, **108**, 014301.
151 M. Farhat, S. Enoch, S. Guenneau and A. B. Movchan, Broadband cylindrical acoustic cloak for linear surface waves in a fluid, *Phys. Rev. Lett.*, 2008, **101**, 134501.
152 H. Y. Chen, J. Yang, J. Zi and C. T. Chan, Transformation media for linear liquid surface waves, *Europhys. Lett.*, 2009, **85**, 24004.
153 Y. A. Urzhumov and D. R. Smith, *Phys. Rev. Lett.*, 2011, **107**, 074501.
154 S. Zhang, D. A. Genov, C. Sun and X. Zhang, Cloaking of matter waves, *Phys. Rev. Lett.*, 2008, **100**, 123002.
155 A. Greenleaf, Y. Kurylev, M. Lassas and G. Uhlmann, Approximate quantum cloaking and almost-trapped states, *Phys. Rev. Lett.*, 2008, **101**, 220404.
156 D. H. Lin and P. G. Luan, Cloaking of matter waves under the global Aharonov–Bohm effect, *Phys. Rev. A: At., Mol., Opt. Phys.*, 2009, **79**, 051605.
157 V. V. Cheianov, V. Fal'ko and B. L. Altshuler, The focusing of electron flow and a Veselago lens in graphene p–n junctions, *Science*, 2007, **315**, 1252–1255.
158 D. A. B. Miller, On perfect cloaking, *Opt. Express*, 2006, **14**, 12457–12466.
159 F. G. Vasquez, G. W. Milton and D. Onofrei, Active exterior cloaking for the 2D Laplace and Helmholtz equations, *Phys. Rev. Lett.*, 2009, **103**, 073901.
160 A. A. Zharov, I. V. Shadrivov and Y. S. Kivshar, Nonlinear properties of left-handed metamaterials, *Phys. Rev. Lett.*, 2003, **91**, 037401.
161 V. M. Agranovich, Y. R. Shen, R. H. Baughman and A. A. Zakhidov, Linear and nonlinear wave propagation in negative refraction metamaterials, *Phys. Rev. B: Condens. Matter Mater. Phys.*, 2004, **69**, 165112.
162 Y. M. Liu, G. Bartal, D. A. Genov and X. Zhang, Subwavelength discrete solitons in nonlinear metamaterials, *Phys. Rev. Lett.*, 2007, **99**, 153901.
163 J. B. Pendry, Time reversal and negative refraction, *Science*, 2008, **322**, 71–73.
164 P. Y. Chen, M. Mohamed and A. Alu, Bistable and self-tunable negative-index metamaterial at optical frequencies, *Phys. Rev. Lett.*, 2011, **106**, 105503.
165 I. V. Shadrivov, S. K. Morrison and Y. S. Kivshar, Tunable split-ring resonators for nonlinear negative-index metamaterials, *Opt. Express*, 2006, **14**, 9344–9339.
166 M. W. Klein, C. Enkrich, M. Wegener and S. Linden, Second-harmonic generation from magnetic metamaterials, *Science*, 2006, **313**, 502–504.
167 A. Rose, D. Huang and D. R. Smith, Controlling the second harmonic in a phase-matched negative-index metamaterial, *Phys. Rev. Lett.*, 2011, **107**, 063902.
168 A. R. Katko, S. Gu, J. P. Barrett, B. I. Popa, G. Shvets and S. A. Cummer, Phase conjugation and negative refraction using nonlinear active metamaterials, *Phys. Rev. Lett.*, 2010, **105**, 123905.
169 S. Palomba, S. Zhang, Y. Park, G. Bartal, X. B. Yin and X. Zhang, Optical negative refraction by four-wave mixing in thin metallic nanostructures, *Nat. Mater.*, 2012, **11**, 34–38.
170 M. Lapine, I. V. Shadrivov, D. A. Powell and Y. S. Kivshar, Magnetoelastic metamaterials, *Nat. Mater.*, 2011, **11**, 30–33.
171 A. Fang, Th. Koschny, M. Wegener and C. M. Soukoulis, Self-consistent calculation of metamaterials with gain, *Phys. Rev. B: Condens. Matter Mater. Phys.*, 2009, **79**, 241104.
172 S. Wuestner, A. Pusch, K. L. Tsakmakidis, J. M. Hamm and O. Hess, Overcoming losses with gain in a negative refractive index metamaterial, *Phys. Rev. Lett.*, 2010, **105**, 127401.
173 S. M. Xiao, V. P. Drachev, A. V. Kildishev, X. J. Ni, U. K. Chettiar, H. K. Yuan and V. M. Shalaev, Loss-free and active optical negative-index metamaterials, *Nature*, 2010, **466**, 735–738.
174 M. T. Hill, *et al.*, Lasing in metallic-coated nanocavities, *Nat. Photonics*, 2007, **1**, 589–594.
175 M. A. Noginov, G. Zhu, A. M. Belgrave, R. Bakker, V. M. Shalaev, E. E. Narimanov, S. Stout, E. Herz, T. Suteewong and U. Wiesner, Demonstration of a spaser-based nanolaser, *Nature*, 2009, **460**, 1110–1112.
176 R. F. Oulton, V. J. Sorger, T. Zentgraf, R. M. Ma, C. Gladden, L. Dai, G. Bartal and X. Zhang, Plasmon lasers at deep subwavelength scale, *Nature*, 2009, **461**, 629–632.
177 Y. Yang, A. Q. Liu, L. K. Chin, X. M. Zhang, D. P. Tsai, C. L. Lin, C. Lu, G. P. Wang and N. I. Zheludev, Optofluidic waveguide as a transformation optics device for lightwave bending and manipulation, *Nat. Commun.*, 2012, **3**, 651.
178 Q. K. Liu, Y. X. Cui, D. Gardner, X. Li, S. L. He and I. I. Smalyukh, Self-alignment of plasmonic gold nanorods in reconfigurable anisotropic fluids for tunable bulk metamaterial applications, *Nano Lett.*, 2010, **10**, 1347–1353.
179 A. B. Golovin and O. D. Lavrentovich, Electrically reconfigurable optical metamaterial based on colloidal dispersion of metal nanorods in dielectric fluid, *Appl. Phys. Lett.*, 2009, **95**, 254104.

